ATLAS Internal Note
PHYS-No-122
23rd April 1998

Consequences of Baryonic R-parity Violation for Measurements of SUSY Particles using the ATLAS Detector

KUNGL TEKNISKA HÖGSKOLAN

Jesper Söderqvist[a]

Physics Department Frescati,KTH
Frescativägen 24, S-104 05 Stockholm, Sweden

Abstract

The discrete R-parity symmetry in SUSY models makes the lightest supersymmetric particle (LSP) stable. It therefore escapes detection and gives the 'traditional' SUSY signature of missing transverse energy. There is, however, no fundamental symmetry to protect R-parity and it may, therefore, be violated naturally. If R-parity is violated, the LSP decays and the missing transverse energy signal decreases significantly or disappears. The final state signatures for SUSY change drastically in such scenario. This note investigates the experimental consequences of baryonic R-parity violation that lead to the decay of the LSP into three jets. We examine the phenomenology defined by the minimal supergravity (SUGRA) model, with the values of the fundamental parameters: $m_0 = 100$ GeV, $m_{1/2} = 300$ GeV, $A_0 = 0$ GeV, $\mu > 0$ and $\tan\beta = 2.1$ (this is the so-called Point 5). The possibility to observe SUSY and reconstruct the LSP and other SUSY particles is demonstrated. It is shown that for this model several precise measurements can be performed that greatly constrain the fundamental parameters of the SUSY model. Potential SUSY discovery and reconstruction of the LSP are also discussed for a few other SUSY models (Points 1,2,3 and 4).

[a] jesper@particle.kth.se

page intentionally left blank

1 Introduction

In the most favoured scenarios for supersymmetry (SUSY) the lightest SUSY particle (LSP) is stable, due to the conservation of a discrete quantum number called R-parity [1]. R-parity is, however, not protected by gauge invariance or any other fundamental symmetry and may, therefore, be naturally violated. The phenomenological success of SUSY, and main the reason for introducing SUSY, i.e. the cancellation of quadratic divergences of the Higgs mass perturbative corrections, still holds even if R-parity is violated. If R-parity is violated the LSP may decay and the experimental signatures differ drastically from those previously studied in ATLAS [2].

The potential of ATLAS to measure SUSY particles is described in a serie of ATLAS notes [3, 4, 5, 6] and in [7, 8]. All of these studies were based on 5 points in the parameter space of the minimal supergravity inspired supersymmetric model (SUGRA) and all assumed that R-parity is conserved. Each point can be described by 5 parameters, as shown in table 1. In this note, we aim to follow on naturally from the results presented

Point	m_0 (GeV)	$m_{\frac{1}{2}}$ (GeV)	A_0 (GeV)	$\tan\beta$	sgn μ	σ_{susy} (pb)
1	400	400	0	2.0	+	3.4
2	400	400	0	10.0	+	3.3
3	200	100	0	2.0	−	1365.0
4	800	200	0	10.0	+	27.1
5	100	300	300	2.1	+	19.2

Table 1: The parameters describing the five SUGRA points and the SUSY cross-section at each point, derived from `ISAJET` (version 7.22) [9].

at the LHCC workshop [10] and investigate the phenomenology if R-parity is violated ($\not{R}$) and experimental consequences for precision SUSY measurements with $\not{R}$ interactions included in the SUGRA model.

In SUGRA models the lightest neutralino, $\tilde{\chi}_1^0$, is LSP. It does not decay due to the conservation of R-parity (R), which follows from the conservation of lepton-number (L) and baryon-number (B). The quantum number R can be defined as :

$$R = (-1)^{3B+L+2S}, \tag{1}$$

where B represents baryon number, L represents lepton number and S is spin. Under this definition, R is +1 for ordinary particles and -1 for SUSY particles. The LSP is therefore stable and needs to be neutral due to cosmological considerations. To conserve R-parity, SUSY particles are always pair-produced, so every SUSY event will contain two $\tilde{\chi}_1^0$'s in the final state, that cannot be directly detected. This gives rise to the classic transverse missing energy signature of supersymmetry. In this note R-parity is assumed to be explicitly broken, so the $\tilde{\chi}_1^0$ decays into three jets. Baer *et al.* [11] have reported on the general implications of the reach of SUSY searches at the LHC for a SUGRA model that includes $\not{R}$ interactions, using the standard cuts for SUSY searches with R-parity

conserved. Here we will try out techniques to measure masses of SUSY particles. These measurements can then be used to constrain the global parameters of the SUGRA model.

This note is organized as follows: Section 2 details the implementation of $\not{R}$ decays. Sections 3 and 4 describe the event generators, detector simulation used in this study. Section 5 discuss the characteristics of Point 5, including masses and branching ratios, and the experimental consequences of R-parity. Secition 6 presents inclusive signatures of $\not{R}$ SUSY and possible initial discovery by suppressing standard model (SM) backgrounds. Exclusive reconstruction using only leptons is demonstrated in section 7. The reconstruction of the $\tilde{\chi}_1^0$ is investigated in section 8. Section 9 presents techniques for direct reconstruction of several other SUSY particles. The reconstruction of the $\tilde{\chi}_1^0$ for a few other SUGRA models (Point 1, 2, 3 and 4) is discussed in section 10. The measurements are summarised and their constraints on the SUGRA parameters are evaluated in section 11. Finally conclusions are drawn in section 12.

2 R-parity Violating Interactions

R-parity follows from lepton (L) and baryon (B) quantum number conservation. By definition, each $\not{R}$ coupling will also violate either L or B quantum numbers. Conservation of R-parity is elegant since there is no problem with rapid proton decays and the $\tilde{\chi}_1^0$ is an ideal candidate for cold dark matter [12]. The $\not{R}$ interactions are however allowed by gauge invariance. Since there is no symmetry that protects R-parity these interactions may occur naturally. In models with a minimal field content, the pertinent $\not{R}$ part of the superpotential is :

$$W_{\not{R}} = \sum_{i,j,k} \overbrace{\lambda_{ijk}\,\widehat{L}_i\,\widehat{L}_j\,\widehat{E}_k}^{\not{L}\Rightarrow e+\nu_\mu\to\tilde{e}} + \underbrace{\lambda'_{ijk}\,\widehat{L}_i\,\widehat{Q}_j\,\widehat{D}_k}_{\not{L}\Rightarrow u+\bar{d}\to\bar{e}} + \overbrace{\lambda''_{ijk}\,\widehat{U}_i\,\widehat{D}_j\,\widehat{D}_k}^{\not{B}\Rightarrow \bar{u}+\bar{d}\to\tilde{d}}, \qquad (2)$$

where : $\widehat{L}$, $\widehat{Q}$, $\widehat{E}$, $\widehat{U}$ and $\widehat{D}$ are superfields representing lepton and quark doublets; charged lepton, up and down quark singlets. The indices, i, j and k, represent generations. The λ (λ'') is antisymmetric under the interchange of the first (last) two indices. The $\not{R}$ interactions add 45 free parameters to the minimal supersymmetric standard model (MSSM) and SUGRA. Equation 2 shows that the first and second terms lead to L violating interactions and examples are given. The final term in equation 2 gives rise to B violating interactions. The different decays of the $\tilde{\chi}_1^0$ due to these interactions are sketched in figure 1. To avoid the tree-level diagrams that allow the proton to decay faster than the experimental bounds [13, 14], it is usually assumed that either the L-violating (λ or λ') terms or the B-violating (λ'') term exist, but not both at once. The limits on L-violating couplings are generally stricter than the limits of the B-violating couplings. A summary of the present experimental limits for the $\not{R}$ couplings are found in reference [14].

In this note we assume an explicit breaking of R-parity due to only one non-zero coupling where the only effect is that the $\tilde{\chi}_1^0$ decays promptly [15]. Production of SUSY particles and other SUSY decays are not affected. The experimental scenarios at the LHC with spontaneous R-parity breaking are discussed in [16]. For those models discussed the dominating effect is also the decay of the $\tilde{\chi}_1^0$.

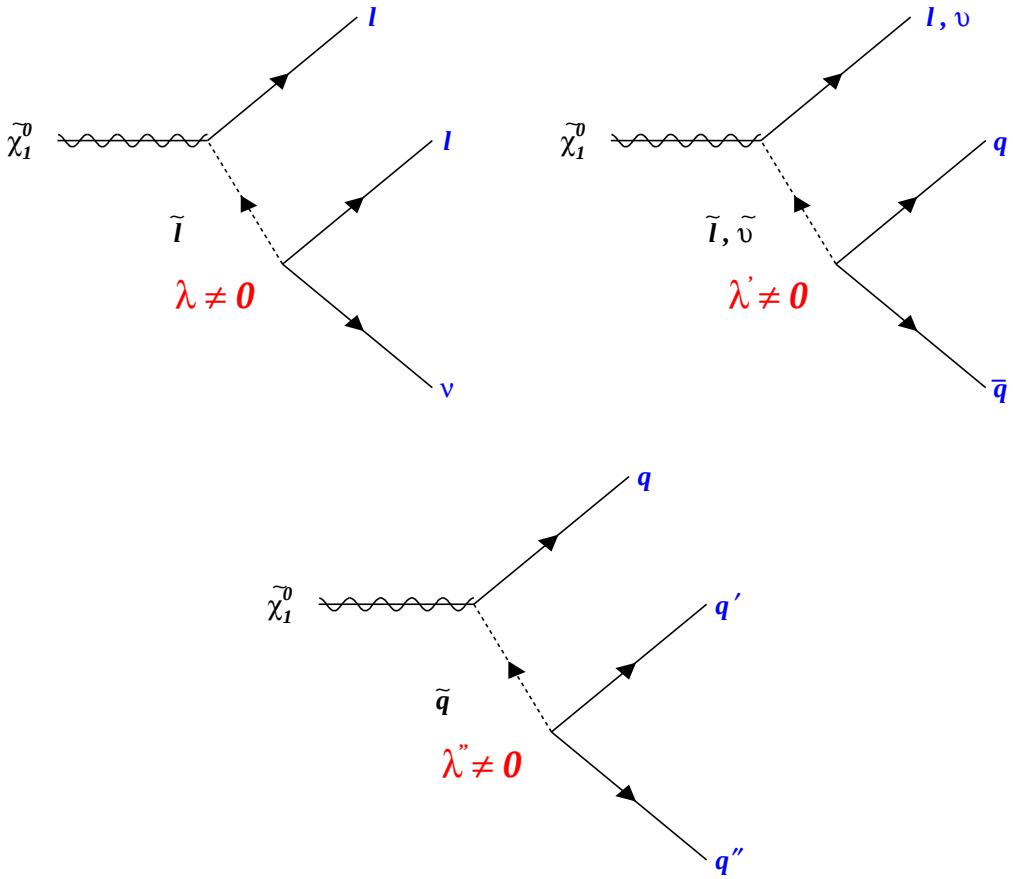

Figure 1: Decays of $\tilde{\chi}_1^0$ due to R-parity violating interactions. Upper left diagram: L-violating interaction from the term $\widehat{\mathrm{L}}_\mathrm{i}\,\widehat{\mathrm{L}}_\mathrm{j}\,\widehat{\mathrm{E}}_\mathrm{k}$; upper right diagram: L-violating interaction from the term $\widehat{\mathrm{L}}_\mathrm{i}\,\widehat{\mathrm{Q}}_\mathrm{j}\,\widehat{\mathrm{D}}_\mathrm{k}$; and lower diagram: B-violating interaction from the term $\widehat{\mathrm{U}}_\mathrm{i}\,\widehat{\mathrm{D}}_\mathrm{j}\,\widehat{\mathrm{D}}_\mathrm{k}$.

It should be noted that the $\tilde{\chi}_1^0$ may have a lifetime which could alter the phenomenology. From cosmological observations, bounds on allowed life times may be extracted that either give the LSP a lifetime much longer than the Universe or less than 1 s [14, 17, 18]. These limits are, however, model dependent. For the former range, the $\tilde{\chi}_1^0$ will always decay outside the detector and the collider signal will be the same as in the R-parity conserved scenario. For the latter range, a fraction of the $\tilde{\chi}_1^0$ particles decay inside the detector and may produce displaced vertices, which should give a peculiar and distinct signature. It should be noted that if R-parity is violated there are several candidates for the LSP and need not be the $\tilde{\chi}_1^0$, since it could be both charged or even a coloured particle. Other phenomenologies are thus possible but the chosen scenario will give an indication of ATLAS capabilities to measure multiple jet signatures.

In the favourable case where L-violating interactions yield $\tilde{\chi}_1^0 \rightarrow \ell_\mathrm{i}\ell_\mathrm{j}\nu$, each SUSY event will contain at least four charged leptons and can easily be separated from SM backgrounds [19]. However, one needs, to evaluate the precision of the measurements of SUSY particle masses and branching ratios that can be performed. If the second L-

violating coupling λ' is non-zero, the $\tilde{\chi}_1^0$ may decay by either $\tilde{\chi}_1^0 \to qq\ell$ or $\tilde{\chi}_1^0 \to qq\nu$. The former decay with a single lepton gives a clear signal above SM backgrounds. However, if the $\tilde{\chi}_1^0$ decays to a neutrino and two jets the visible final state is hadronic and, as the p_T from the ν is much softer than from an escaping $\tilde{\chi}_1^0$, the signal suffers from large SM backgrounds at the same time as the $\tilde{\chi}_1^0$ cannot be fully reconstructed. This scenario deserves a special study. The last B-violating term yields a decay $\tilde{\chi}_1^0 \to q_i q_j q_k$. This is also considered to be a difficult experimental scenario since the $\tilde{\chi}_1^0$ decays into three jets with a potentially large QCD background. The flavours of jets which the $\tilde{\chi}_1^0$ can decay into, depending on which λ'' coupling is non-zero, is listed in table 2. Given the large

	$\tilde{\chi}_1^0 \to$		$\tilde{\chi}_1^0 \to$		$\tilde{\chi}_1^0 \to$
λ''_{112}	u d s	λ''_{212}	c d s	λ''_{312}	t d s
λ''_{113}	u d b	λ''_{213}	c d b	λ''_{313}	t d b
λ''_{123}	u s b	λ''_{223}	c s b	λ''_{323}	t s b

Table 2: The different decay modes of the $\tilde{\chi}_1^0$ for different λ'' couplings.

number of possible couplings in, the only source of $\not{R}$ interactions is assumed to come from a non-zero λ''_{212} coupling in the superpotential. The $\tilde{\chi}_1^0$ therefore decays:

$$\tilde{\chi}_1^0 \to c\,d\,s \text{ or } \bar{c}\,\bar{d}\,\bar{s}, \tag{3}$$

with a branching ratio of 50% for each mode. This is chosen as the relevant coupling since it has no significant experimental bound [13, 14]. This all-hadronic $\tilde{\chi}_1^0$ decay was simulated within the SUGRA model. The presence of c-jets gives a very challenging experimental scenario due to the 10% probability of mis-tagging them as b-jets. Therefore key signatures, such as $h^0 \to b\bar{b}$, may be more difficult to extract in this case.

3 Event Generation and Detector Simulation

3.1 Overview

SUSY processes were generated with the `ISAJET` (version 7.31) [9] Monte Carlo package. The decay of the $\tilde{\chi}_1^0$ was simply introduced using the `FORCE` datacard. Standard Model background processes ($t\bar{t}$, W+jets, Z+jets) were generated with the `PYTHIA` (version 5.710) Monte Carlo package [20], where `JETSET` (version 7.405) was used for the hadronization processes. QCD background was generated with `HERWIG` (version 5.9) [21].

The detector response was simulated using the `ATLFAST` (version 1.21) package [22]. This allows events to be analysed using a fraction of the computing overhead needed for a full simulation. Jet reconstruction in the calorimeters, momentum and energy smearing for leptons and photons and missing transverse energy are all simulated and agree well with results from full simulations [23]. It should be noted that `ATLFAST` is designed to be interfaced to `PYTHIA` and a well-tested private interface to `ISAJET` was used. Also, `ATLFAST` needed several fixes to give stable performance with the higher jet multiplicities

intrinsic to hadronic decay modes of the $\tilde{\chi}_1^0$ [b]. Full details about ATLFAST can be found in the reference [22], only a brief overview of features related to the analysis presented in this note are described below.

3.2 Isolated Leptons

The lepton must fall within the detector acceptance, $|\eta_{e,\mu}| < 2.5$, and the minimum electron and muon transverse energy used in this analysys is 10 GeV. Leptons are isolated if they are separated by ΔR>0.4 from other clusters and have an accompanying transverse energy of less than 10 GeV in a 'cone' of ΔR=0.2 around the lepton ($\Delta R = \sqrt{(\Delta\eta)^2 + (\Delta\phi)^2}$).

3.3 Jet Reconstruction

SUSY decays give high jet multiplicity. The reconstruction of final states that include many jets is extremely difficult and is an area that will require much attention to study and master when real data become available. The hadronic decays of the $\tilde{\chi}_1^0$ produce an even more difficult experimental situation than any scenario previously considered.

In this study the reconstruction of jets was tried with two different jet finders: the standard 'cone' algorithm, which is implemented in ATLFAST[c], and a new algorithm called 'mulguisin' [24][d] developed by I. Parkic.

3.3.1 Cone Cluster Algorithm

The 'cone' algorithm reconstructs jets by forming a cone, of fixed size, around an initiator cell containing the maximum energy. The procedure for finding jets is as follows. Cells with transverse energy greater than a threshold (E_T^{init} >1.5 GeV), in order of decreasing E_T, are taken as possible initiators of clusters and cells within ΔR are included in the cluster. Clusters are formed until there are no initiator cells left. If two jets are overlapping, the energy in shared cells is divided between the two clusters weighted by the jet-energy. After this sharing the jet directions are not recomputed in the analysis presented here.

3.3.2 Mulguisin Cluster Algorithm

The 'mulguisin' algorithm [24] has a flexible cone size with a minimum size here called resolution (R_0). For this analysis R_0=0.25 is used. Reconstruction of jets is an iterative procedure:

1. Find the maximum E_T cell and define it as the first cluster. Set initial cluster size to R_0.

2. Find the next cell in order of decreasing E_T.

[b] Many of these fixes have been included in later releases of ATLFAST.
[c] Implemented in subroutine MAKCLU
[d] The name originates from an old Korean tale about ghosts living in a sea. (*mul=water, guisin=ghost*)

3. Calculate the distance between the cell and the nearest cluster
   a. If the distance is smaller than the cluster size, i.e. inside the cluster region, attach the cell to this cluster. Recompute the cluster center weighted by the cells now included in the cluster and the cluster size.
   b. If the distance is greater than the cluster size, i.e. outside the cluster region, define a new cluster with initial size R_0.

4. Go to step 2 until there are no cells left

Step 3a can be summarised:

$$\begin{aligned} \mathrm{E}^{clus}_{T\,k+1} &= \mathrm{E}^{clus}_{T\,k} + \mathrm{E}^{cell}_{T\,i} \\ \eta^{clus}_{k+1} &= (\mathrm{E}^{clus}_{T\,k}\eta^{clus}_{k} + \mathrm{E}^{cell}_{T\,i}\eta^{cell}_{i})/(\mathrm{E}^{clus}_{T\,k} + \mathrm{E}^{cell}_{T\,i}) \\ \phi^{clus}_{k+1} &= (\mathrm{E}^{clus}_{T\,k}\phi^{clus}_{k} + \mathrm{E}^{cell}_{T\,i}\phi^{cell}_{i})/(\mathrm{E}^{clus}_{T\,k} + \mathrm{E}^{cell}_{T\,i}) \\ \mathrm{R}^{clus}_{k+1} &= max(\mathrm{R}^{clus}_{k}, \delta) \end{aligned} \tag{4}$$

where δ is the distance from the cluster center to the cell furthest away in the cluster. This procedure is similar to the 'cone' algorithm, but cells are added one by one to the cluster. Each cell of the calorimeter is assigned to some cluster. The shape of the clusters are not necessarily circles. In the present implementation no cells are shared by clusters. Jets can be closer and still be resolved since the initial cone used is smaller than in the 'cone' algorithm.

3.3.3 Definition of Jets, Flavour Tagging and Recalibration

In both clustering algorithms, cells assigned to the electromagnetic clusters that reconstruct isolated leptons (and photons) are not re-used. In the present analysis the cluster energy must exceed at least 17.5 GeV to be accepted as a jet. This threshold has been varied between 15-25 GeV to verify the dependence of the results on the threshold.

A jet is marked as originating from a bottom(charmed) hadron if the momentum vector of a primary b(c) quark of transverse momenta (after final state radiation (FSR)) is greater than 5 GeV, and has $|\eta| < 2.5$, and points to the jet within $\Delta\mathrm{R}< 0.2$. An additional random tagging is applied to simulate the expected ATLAS tagging efficiencies.

A jet may have a transverse spread larger than the cone used for the reconstruction so that energy is lost outside the cone or neutrinos produced in the shower escape with a fraction of the actual jet energy. The latter is mainly important for heavy flavour quarks. Therefore the jet energies need to be recalibrated to yield a value of the initial parton energy . The p_T dependent calibration factors can be applied as shown in [22]. Reference [24] shows that the 'mulguisin' calibration factors are smaller and less dependent on the p_T, but one should note that it will be much harder to understand the calibration procedure due to the varying cone size. However, recalibration of single jets event by event will significantly drop the reconstruction efficiency when jets overlap, since reconstructed jets may have contributions from several real jets. Invariant masses are therefore formed from jets that are not recalibrated and are thus slightly off from their nominal values. The determination of their absolute position with real data will rely on comparison with Monte Carlo samples.

3.4 Supplementary Jet and Lepton Selection Criteria

The jets reconstructed are grouped into three classes : b jets, c jets and light (u,d,s or gluon) jets. The tagging procedure is detailed in the previous section. For the analysis in this work the following criteria were used to emulate the ATLAS tagging efficiencies for b jets and rejection of other jets.

- Probability to identify a b jet as a b jet is 60 %.
- Rejection against c-jets is a factor of 10.
- Rejection against other jets is a factor of 100.
- Probability to identify a τ lepton is 30 %.

The first three criteria were taken from [25] and the final criterion was taken from [26][e]. The reconstruction efficiency for leptons was defined as 90 % for both isolated muons and electrons. Finally, to ensure a good quality sample, light jets and b jets (leptons) were required to have transverse momenta exceeding at least 17.5 GeV (10 GeV). The jet threshold was, however, varied between 15-25 GeV to check its influence on the reconstruction efficiency.

3.5 Example Event

The cells of the central calorimeter for a typical $\not{R}$ SUSY event with reconstructed jets are plotted in figure 2, where the 'cone' jet finder is used, and in figure 3, where "mulguisin" is used. The circles indicate reconstructed jets and isolated leptons (bold circles). The circles show which cells are included in each jet. Note, that for 'mulguisin' the circles are a bit misleading since the radius of the circle is the distance to the furthest cell from the barycenter included in the jet but not all cells in this cone are included. The numbers in the circles are the reconstructed transverse jet momenta. The larger digits are for jets that are used in the $\tilde{\chi}_1^0$ reconstruction (discussed in section 8.2). Note that the 'mulguisin' has a flexible cone size and jets that are close together can in principle be better resolved .A $\eta - \phi$ lego plot with the energy in each cell of the calorimeter is shown in figure 4. From visual inspection one can identify the jets that are close together. The jets are narrow since there is no transverse shower spreading, which is one of the inherent weaknesses of particle level simulation. The reconstruction efficiencies and resulting jet multiplicities for the two jet finders are further discussed in section 5.1.

[e]The process $A^0 \to \tau^+\tau^-$ was investigated. We assume the same τ mis-identification.

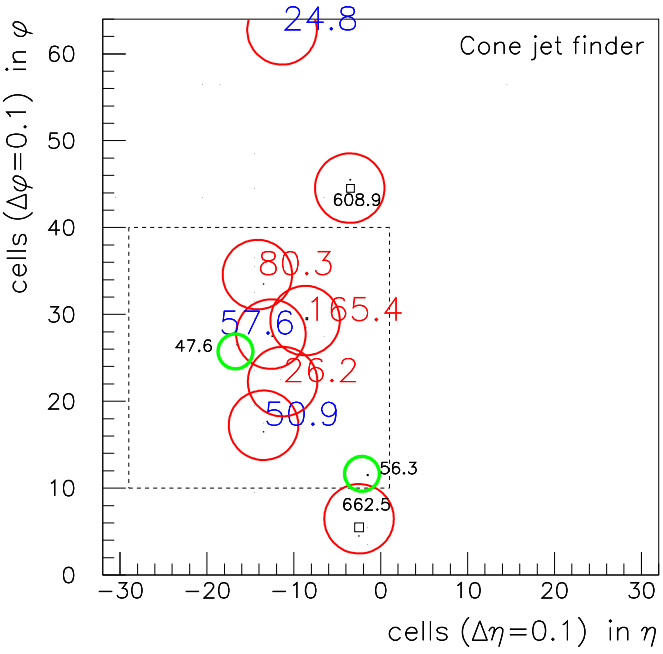

Figure 2: A calorimeter map in $\eta - \phi$, where the size of the boxes are proportional to the energy in the cell. Circles are jets reconstructed with the 'cone' algorithm and isolated leptons. The numbers in the circles are the reconstructed transverse jet momenta in GeV. The larger digits are for jets that are used in the $\tilde{\chi}_1^0$ reconstruction (discussed in section 8.2). Note that the forward calorimeters, $|\eta|$ >3.2, are not included. The calorimeter cells in the dashed square are shown zoomed in figure 4.

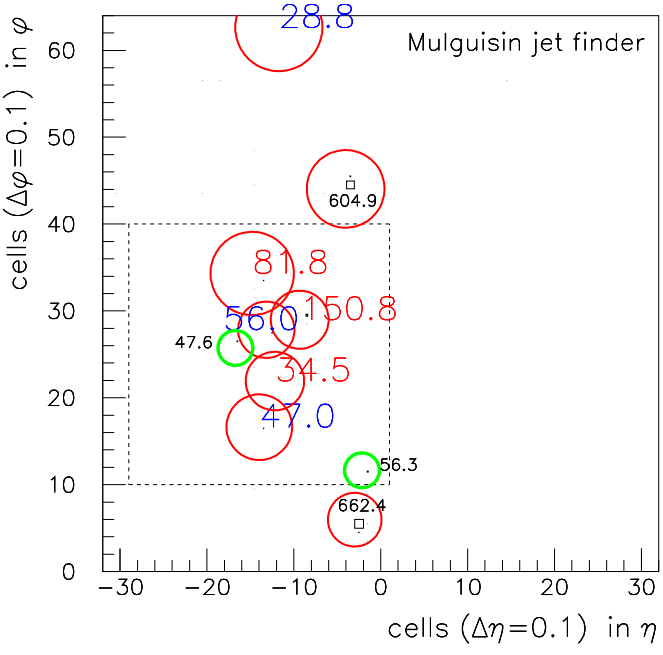

Figure 3: Same calorimeter map in $\eta - \phi$ as in figure 2. Circles are jets reconstructed with the 'mulguisin' algorithm and isolated leptons.

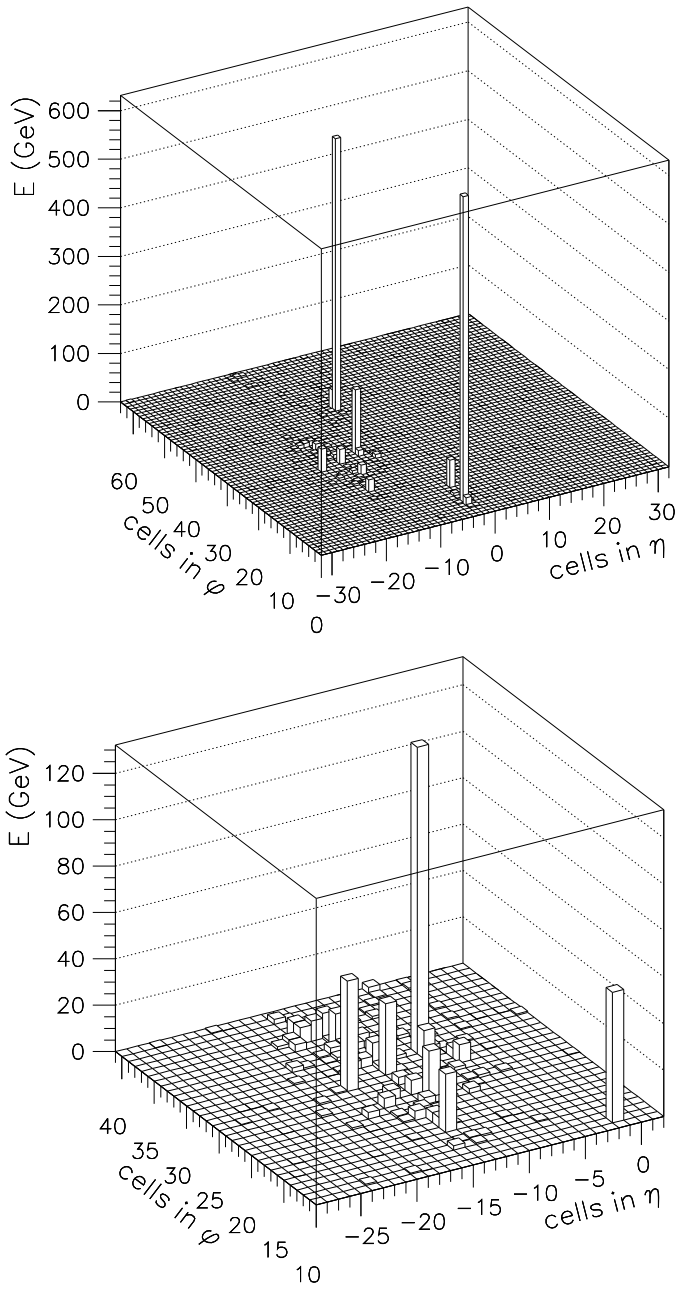

Figure 4: A lego plot of the calorimeter in $\eta - \phi$, for the same event as in figures 2 and 3, where the height of the histogram is proportional to the energy in the cell. The top plot shows the whole central calorimeter and the lower plot is a zoom in of the indicated region in figure 2 and 3, which have many close jets.

4 Experimental Sensitivity

The sensitivity of the exclusive reconstructions was estimated in the following way. The parameters of the model were frozen and all masses kept at their nominal values except for one SUSY particle mass, which was varied. Then the statistical sensitivity of the kinematic distribution under study was estimated using a Kolmogorov test [27]. The quoted uncertainties are 1 σ experimental errors. The systematic uncertainties were estimated from the following assumptions:

- the absolute energy scale will be known at least to 0.1% for electrons and muons, and to better than 1.0% for hadronic jets [28].
- the systematic uncertainty on cross-section measurements was taken to be 15% [3] (e.g. in the case of the semi-inclusive measurements of the rate of four jets in section 6.3).

The final errors quoted are therefore estimates of ATLAS experimental capabilities to measure SUSY particles. The interpretation of the results will however rely on comparison with a Monte Carlo model.

5 Characteristics of Point 5

The phenomenology of Point 5 offers a wide variety of signals and was therefore chosen as a testbench for the R-parity violating analysis. The fundamental SUGRA parameters that define the model are given in table 1. A selection of sparticle masses are listed in table 3. For the LHCC study, this point was chosen in a region that is favoured from

Sparticle	Mass (GeV)	Sparticle	Mass (GeV)
$\tilde{q}_L$	687	$\tilde{g}$	767
$\tilde{q}_R$	664	$\tilde{\chi}_2^0$	233
$\tilde{t}_1$	494	$\tilde{\chi}_1^0$	122
$\tilde{t}_2$	706	$\tilde{\chi}_1^\pm$	232
$\tilde{b}_1$	634	$\tilde{\chi}_2^\pm$	526
$\tilde{b}_2$	662	h^0	95
$\tilde{\ell}_R$	157	A^0	613
$\tilde{\ell}_L$	239	H^0	618

Table 3: Sparticle masses at SUGRA point 5 using `ISAJET` (version 7.31).

cosmological considerations. To get the correct relic density of neutralino dark matter, $\tilde{\chi}_1^0$ annihilations through relatively light virtual sleptons must occur such as not to overclose the universe [17, 18, 29]. This argument is, of course, not valid if the lightest neutralino decays.

The mass of the lightest Higgs boson is just within the range for a possible discovery by LEP 2. The left and right handed squarks of the first two generations are split by 23 GeV.

The masses of the first and second generation scalar fermions are nearly mass degenerate. Mixing in the third generation makes the masses of the lighter stop considerably lighter than all other squarks. Notice that the sleptons have moderate masses and that they are produced in a large fraction of the $\tilde{\chi}_2^0$ decays. The dominant branching ratios relevant to the studies that can be performed at LHC are given in table 4. The total SUSY production

Decay			Branching Ratio	Decay			Branching Ratio
$\tilde{\chi}_1^0$	$\rightarrow$	cds	100%	$\tilde{u}_L$	$\rightarrow$	$\tilde{\chi}_2^0 q$	32%
$\tilde{\chi}_2^0$	$\rightarrow$	$\tilde{\chi}_1^0 h^0$	64%	$\tilde{u}_L$	$\rightarrow$	$\tilde{\chi}_1^\pm q$	65%
$\tilde{\chi}_2^0$	$\rightarrow$	$\tilde{\ell}_R \ell$	18%	$\tilde{u}_R$	$\rightarrow$	$\tilde{\chi}_1^0 q$	100%
$\tilde{\chi}_1^+$	$\rightarrow$	$\tilde{\chi}_1^0 W^+$	88%	$\tilde{t}_1$	$\rightarrow$	$\tilde{\chi}_1^0 t$	22%
h^0	$\rightarrow$	$b\bar{b}$	88%	$\tilde{t}_1$	$\rightarrow$	$\tilde{\chi}_2^0 t$	16%
$\tilde{g}$	$\rightarrow$	$\tilde{q}_L q$	24%	$\tilde{t}_1$	$\rightarrow$	$\tilde{\chi}_2^+ t$	62%
$\tilde{g}$	$\rightarrow$	$\tilde{q}_R q$	38%	$\tilde{\ell}_L$	$\rightarrow$	$\tilde{\chi}_1^0 \ell$	94%
$\tilde{g}$	$\rightarrow$	$\tilde{b}_L \bar{b}$	15%	$\tilde{\ell}_R$	$\rightarrow$	$\tilde{\chi}_1^0 \ell$	100%
$\tilde{g}$	$\rightarrow$	$\tilde{b}_R \bar{b}$	10%				
$\tilde{g}$	$\rightarrow$	$\tilde{t}_1 t$	14%				

Table 4: Dominant branching ratios at SUGRA Point 5 from `ISAJET` (version 7.31).

cross-section is approximately 18 pb and in table 5 the cross-sections for different primary processes are given.

Process			Cross-section (pb)
pp	$\rightarrow$	$\tilde{g}\tilde{g}$	1.52
pp	$\rightarrow$	$\tilde{g}\tilde{q}_L$	3.69
pp	$\rightarrow$	$\tilde{g}\tilde{q}_R$	4.02
pp	$\rightarrow$	$\tilde{q}_L\tilde{q}_L$	1.38
pp	$\rightarrow$	$\tilde{q}_L\tilde{q}_R$	2.23
pp	$\rightarrow$	$\tilde{q}_R\tilde{q}_R$	1.62
pp	$\rightarrow$	$\tilde{\ell}\tilde{\ell}$	0.43
pp	$\rightarrow$	$\tilde{t}_1\tilde{t}_1$	0.59
pp	$\rightarrow$	other	2.23
		Total	**17.78**

Table 5: SUSY primary production cross-sections at SUGRA Point 5 calculated with `ISAJET` (version 7.31).

5.1 Experimental Consequences of R-parity Violation

The standard SUSY signature of missing transverse energy ($\not{E}_T$) vanishes if the $\tilde{\chi}_1^0$ decays. Figure 5 compares $\not{E}_T$ from a SUSY signal sample where R-parity is conserved and the

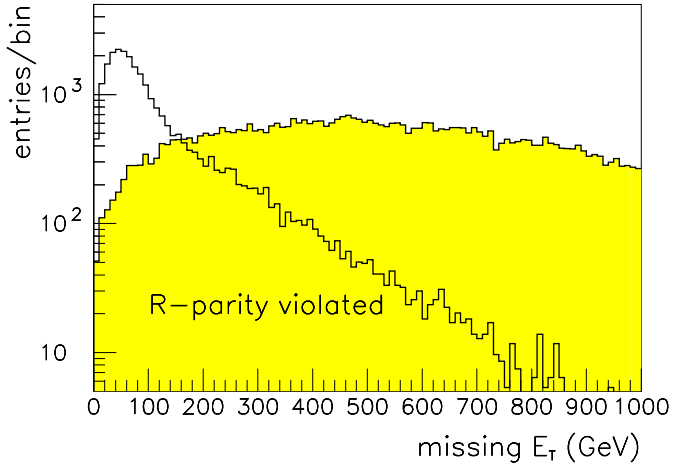

Figure 5: Transverse missing energy for R-parity conserved (shaded) and for R-parity violated at SUGRA Point 5.

baryonic R-parity violated scenario as considered here for Point 5. The $\not{R}$ distribution is, of course, much softer and cannot be used to suppress QCD backgrounds. The jet multiplicity increases by 4.4 units for $\not{R}$ as shown in figure 6 using the mulguisin jet finder. There are six additional jets from the $\tilde{\chi}_1^0$ decay, but some jets are too soft to be

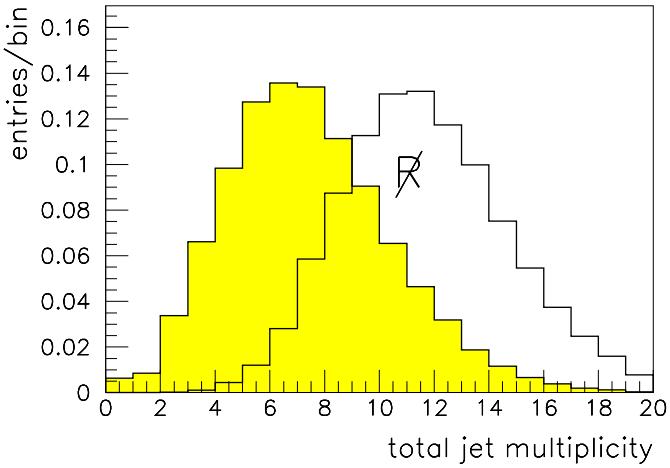

Figure 6: Jet multiplicity for SUGRA Point 5 with and without R-parity conserved as reconstructed with the mulgusin jet finder.

reconstructed, are lost outside the detector acceptance, or overlap with other jets. The lepton multiplicity is reduced by 5.6%, because leptons are lost inside the additional jets from the hadronic $\tilde{\chi}_1^0$ decay. The momentum distributions of the 9 leading jets are plotted in figure 7. Even if the jet spectrum is hard and one could select events with 8 jets with $p_T > 50$ GeV one needs to use events with lower p_T jets for the reconstruction of $\tilde{\chi}_1^0$ and

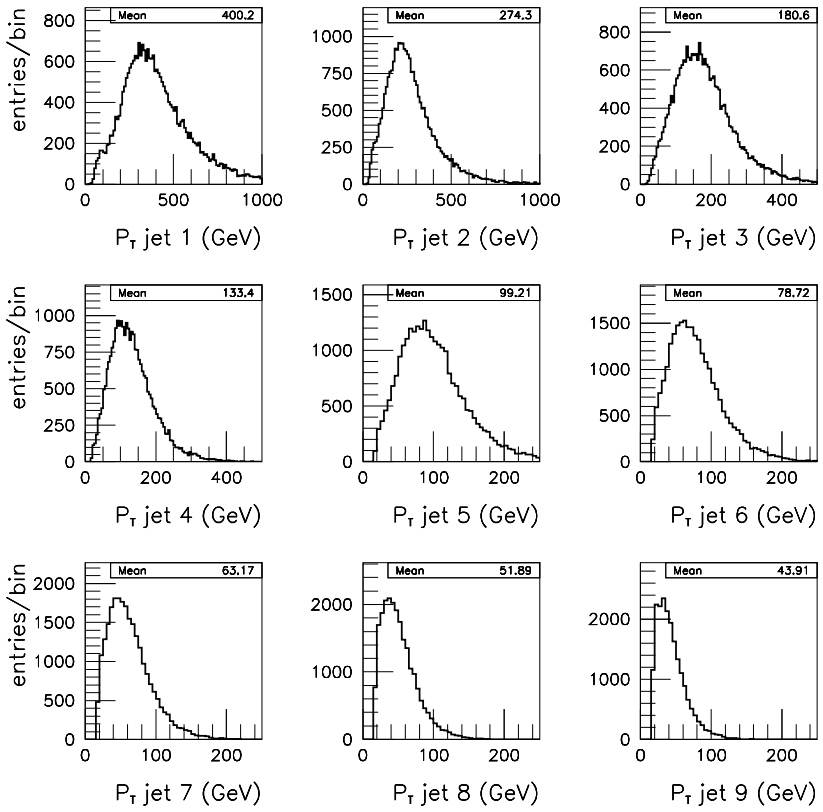

Figure 7: Transverse momentum of the 9 leading jets in order of decreasing p_T for Point 5, where the $\tilde{\chi}_1^0$ decays into 3 jets.

other lighter sparticles, due to the soft spectrum from $\tilde{\chi}_1^0$ decays (see section 8).

5.2 Event samples

For Point 5, there are 534 000 SUSY events expected to be produced after 3 years of running at low luminosity. Almost all the expected statistics of 500 000 signal events was generated. To check the sensitivity of the mass measurements, samples with one particle mass varied at a time were generated. Half of the above statistics were generated for each of these samples.

Cross-sections for SM background processes are given in table 6. Enough events were generated to have weights in the range 5-20 for the various SM processes that may contribute to the background. The number of events in the samples and their weights are given in table 7. Clearly it is impractical to generate even a fraction of the full QCD statistics. Therefore, QCD events were generated in p_T-bins of 100 GeV. Cross-section times cut efficiency for two minimal sets of cuts[f] are shown as a function of the p_T of the 2-2 hard scattering process in figure 8. Only QCD events that come from a hard scatter interaction produce multiple hard jets that pass the event selection. Below 300 GeV

[f]For all exclusive reconstructions stricter, cuts were used.

Process	Kinematic Cut				σ	
QCD	p_T^{2-2}	$>$	10	GeV	5	mb
	p_T^{2-2}	$>$	300	GeV	11	nb
	p_T^{2-2}	$>$	400	GeV	2.6	nb
$t\bar{t}$	p_T^{2-2}	$>$	10	GeV	590	pb
W+jets	p_T^{2-2}	$>$	10	GeV	73	nb
Z+jets	p_T^{2-2}	$>$	10	GeV	28	nb

Table 6: Cross-sections of SM background processes. (p_T^{2-2} - initial momenta of generated 2-2 hard scattering process.)

Process	p_T-range (GeV)	Generated events	Weight	Generator
QCD	p_T^{2-2} <300	$2{\cdot}10^6$	-	Herwig 5.9
	300< p_T^{2-2} <400	$4.7{\cdot}10^6$	17	"
	400< p_T^{2-2} <500	$1.5{\cdot}10^6$	12	"
	500< p_T^{2-2}	$1.8{\cdot}10^6$	2-20	"
$t\bar{t}$	100< p_T^{2-2}	$7{\cdot}10^4$	~ 50	Pythia
W+jets	100< p_T^{2-2}	$1{\cdot}10^5$	~ 300	"
Z+jets	100< p_T^{2-2}	$1{\cdot}10^5$	~ 120	"

Table 7: Event samples for Standard Model background studies.

the probability for QCD events to pass the selection drops abruptly and therefore it was concluded it was sufficient to generate large QCD statistics down to a p_T of 300 GeV for the initial hard scattering. The model used for QCD generation is accepted as a good practical understanding of the topic at present. However, it should be noted that there is a large theoretical uncertainty in the generation of QCD events with this high jet multiplicity. A significantly higher rate has been found for full matrix element calculations[g] compared to parton shower models [30], but one does not know which one is closest to reality. Once real data become available one can measure the actual rate of high jet multiplicity QCD events in a similar way as the properties of 6-jet events have been measured by CDF [31].

6 Inclusive Signatures

6.1 Transverse energy

SUSY production at the LHC is dominated by squarks and gluinos, which decay into hard jets. In the case of R-parity conservation the $\not\!\!E_T$ from escaping $\tilde{\chi}_1^0$'s was combined with the momentum of the four hardest jets to get a quantity that could be used to estimate the mass scale of new physics [2, 8]. To check if this method can be used also here, but

[g]The NJETS Monte Carlo [32] can only calculate the rate for 5 or less jets and could not be used.

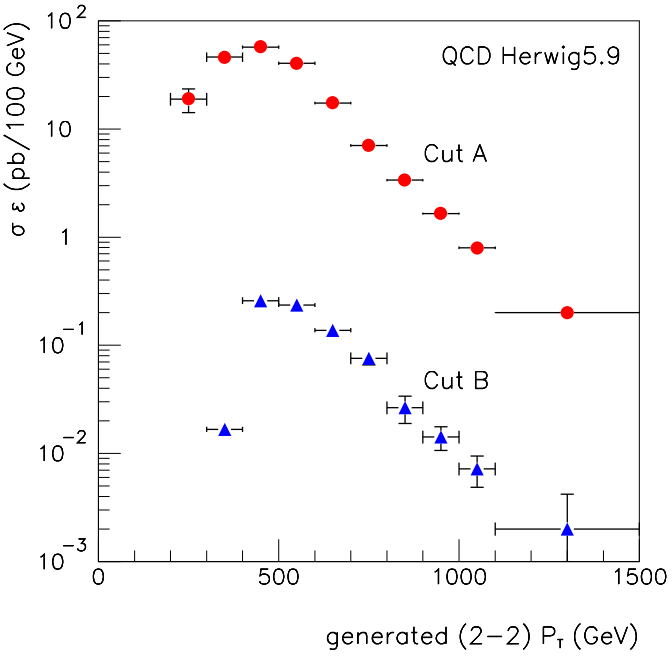

Figure 8: The $\sigma\times$cut-efficiencies versus p_T for hard scattering QCD processes for two sets of cuts. Cut A: 8 jets p_T >17.5 GeV, m_{Tcent} >1000 GeV, circularity>0.2. (m_{Tcent} is defined in section 6.1). Cut B: Cut A and at least 1 lepton with p_T >10 GeV.

with the vanished $\not\!\!E_T$ replaced with multiple jets from the $\tilde{\chi}_1^0$ decay, a global variable of transverse energy is formed as:

$$m_{Tcent} = \sum_{(|\eta| < 2)} p_T^{\text{jet}} + \sum_{(|\eta| < 2)} p_T^{\text{lepton}} \tag{5}$$

A first selection of events is done using the following cuts:

- at least 8 jets with $p_T > 17.5$ GeV
- at least 1 jet with $p_T > 200$ GeV
- circularity > 0.2, thrust < 0.9

For events that pass this selection, m_{Tcent} is calculated. The obtained distribution is plotted in figure 9. The dominating background comes from QCD and is larger by orders of magnitude than the signal throughout the whole range. The SM background from $t\bar{t}$,W+jets and Z+jets is small if the cut $m_{Tcent} > 1000$ GeV is applied. It was checked wheter the jet cuts could be raised to provide an initial discovery by requiring:

- at least 8 jets with $p_T > 50$ GeV

The m_{Tcent} spectrum obtained is shown in figure 10. Even if the generated QCD statistics is poor it it is clear that QCD dominates and additional cuts are needed to increase the signal-to-background ratio. A further requirement ,e.g. the presence of at least 1 lepton in the event, is therefore necessary to extract an inclusive SUSY signal from the QCD multi-jet background.

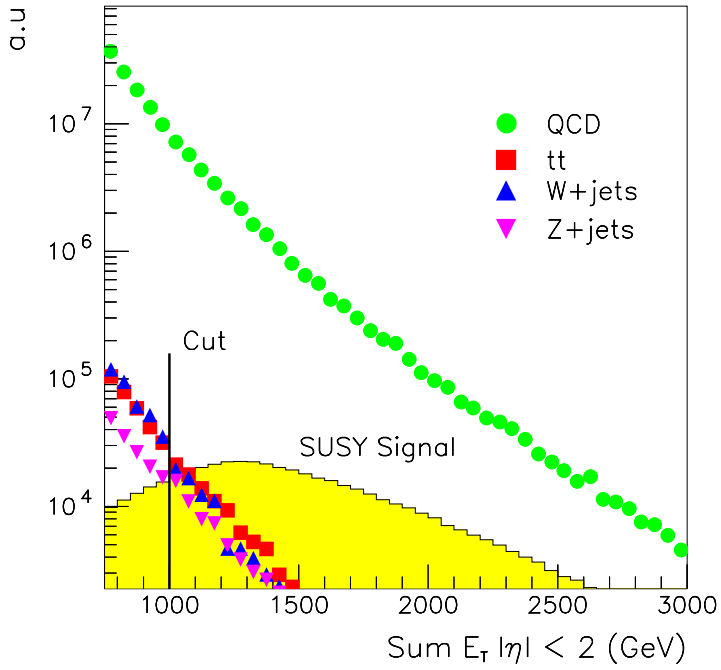

Figure 9: The scalar sum of central jets and isolated leptons for events with at least 8 jets with p_T >17.5 GeV for the inclusive SUSY signal in Point 5 and various SM processes.

6.2 Rate of Leptons

An excess of leptons in events with multiple jets is a classic and robust SUSY signature and thus a natural starting point for the analysis. In general, multiple lepton signals have the best discovery reach in SUGRA models [33]. A preselection was done applying the cuts:

- at least 8 jets with $p_T > 25$ GeV
- at least 1 jet with $p_T > 200$ GeV and a second jet with $p_T > 100$ GeV
- circularity > 0.2, thrust < 0.9
- $m_{Tcent} > 1000$ GeV.

The multiplicity of leptons, with $p_T > 15$ GeV, for this event sample is shown in table 8. By requiring one lepton a signal-to-background of 2.4 is achieved and for two leptons the ratio is greater than 10. No generated background events with 3 or more leptons passed the cut, while 939 SUSY events are expected after 3 years of running at low luminosity.

6.3 Rate of b-jets

Another feature of SUSY events in most of the parameter space is an excess of heavy quark flavours. They may be produced in $\tilde{g}\tilde{g}$, $\tilde{t}\tilde{t}$ or $\tilde{b}\tilde{b}$ production with subsequent decays $\tilde{g} \to \tilde{t}t, \tilde{b}b$, $\tilde{t} \to \tilde{\chi}_i^+ b$ and $\tilde{t} \to \tilde{\chi}_i^0 t$. Another source is light Higgs boson decay $h^0 \to b\bar{b}$.

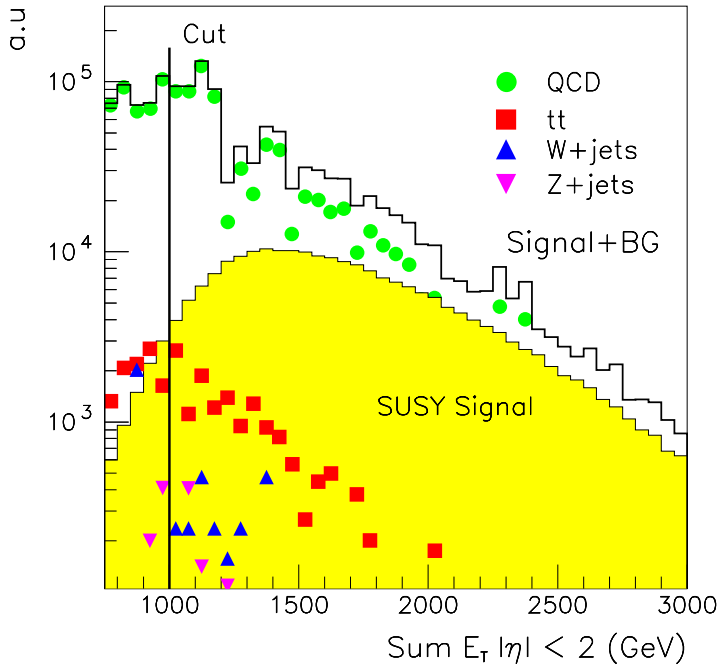

Figure 10: The scalar sum of central jets and isolated leptons for events with at least 8 jets with $p_T^{\text{jets}} > 50$ GeV.

The expected rates of events containing b-jets with p_T >17.5 GeV, using the same cuts as in section 6.1, with and without the requirement of leptons in the event, are given in table 9. Only for 4 b-jets is there a small excess if no lepton is required, but the background estimation is not solid enough to make any firm conclusion at this stage. If events are selected requiring at least 1 or 2 leptons (e, μ), with p_T^{ℓ} >10 GeV, a clear excess of SUSY events can be observed with a comfortable signal-to-background.

The b-jet rate when the p_T-cut is raised to 50 GeV is listed in table 10. The SUSY

Process	$N_\ell \geq 1$	$N_\ell \geq 2$	$N_\ell \geq 3$	$N_\ell \geq 4$	$N_\ell \geq 5$	$N_\ell \geq 6$
SUSY	46097	10363	939	112	2.1	0
QCD	14691	466	< 46	-	-	-
$t\bar{t}$	3800	339	< 25	-	-	-
W+jets	395	< 61	-	-	-	-
Z+jets	114 ± 35	104 ± 34	< 26	-	-	-
total SM	19000	909	< 71	0	0	0
S/B	2.4	11	> 13	-	-	-

Table 8: Expected multiplicities of leptons (e,μ) with $p_T \geq 15$ GeV for an integrated luminosity of $3 \cdot 10^4$ pb^{-1} for the SUSY signal and SM backgrounds. Where no generated Monte Carlo events pass the selection an upper limit at 90% confidence level is given.

Process	Multiplicity of b-jets $p_T^b \geq 17.5$ GeV					
			$N_\ell \geq 1$		$N_\ell \geq 2$	
	$N_b \geq 2$	$N_b \geq 4$	$N_b \geq 2$	$N_b \geq 4$	$N_b \geq 2$	$N_b \geq 4$
SUSY	64655	3805	13567	749	2850	138
QCD	$1.3 \cdot 10^5$	3068	4173	< 46	185 ± 43	-
tt	14800	148 ± 38	1441	< 25	< 25	-
W+jets	868	-	79 ± 45	-	< 61	-
Z+jets	780	2 ± 2	< 276	-	-	-
Total SM	$1.5 \cdot 10^5$	3218	5693	9	< 264	-
S/B	0.4	1.1	2.3	>50	>10	-

Table 9: Expected rate of events with different b-jet multiplicities ($p_T^b \geq 17.5$ GeV) from SUSY and SM physics processes for an integrated luminosity of $3 \cdot 10^4$ pb^{-1}. The leptons (e or μ) are required to have $p_T > 10$ GeV. Where no generated Monte Carlo events pass the selection an upper limit at 90% confidence level is given.

Process	Multiplicity of b-jets $p_T^b \geq 50$ GeV					
			$N_\ell \geq 1$		$N_\ell \geq 2$	
	$N_b \geq 2$	$N_b \geq 4$	$N_b \geq 2$	$N_b \geq 4$	$N_b \geq 2$	$N_b \geq 4$
SUSY	43507	1310	9100	249	1853	44
QCD	$8.4 \cdot 10^4$	62 ± 34	2235	< 46	60 ± 34	-
tt	12501	135 ± 37	1048	< 25	-	-
W+jets	473	-	-	-	-	-
Z+jets	545	2 ± 2	-	-	-	-
total SM	$9.8 \cdot 10^4$	< 249	3283	-	< 94	-
S/B	0.4	> 5.3	2.7	-	>25	-

Table 10: Expected rate of events with different b-jet multiplicities ($p_T^b \geq 50$ GeV) from SUSY and SM physics processes for an integrated luminosity of $3 \cdot 10^4$ pb^{-1}. The leptons (e or μ) are required to have $p_T > 10$ GeV. Where no generated Monte Carlo events pass the selection an upper limit at 90% confidence level is given.

signal with 4 or more b-jets drops by 65% at the same time as the SM background decreases by 94%, resulting in a signal-to-background greater than 5. If such an excess of events with multiple leptons and b-jets was observed one would safely conclude that there is 'New Physics'.

We will now continue with the exclusive reconstruction of SUSY events.

7 Edge in the Dilepton Invariant Mass

Final states with multiple hard leptons offer robust and distinctive signatures. It is therefore natural to use the observed excess of leptons in events with multiple hard jets for exclusive reconstruction. Events are selected requiring:

- at least 8 jets with $p_T > 20$ GeV
- circularity> 0.2, thrust< 0.9
- $m_{Tcent} > 1000$ GeV
- 2 leptons (e, μ), opposite sign (OS) and same flavour (SF) with $p_T^{\ell} > 10$ GeV

The invariant mass of the two OS SF leptons is shown in figure 11. A clear structure with a sharp edge is visible. The combinatorial background where the leptons come

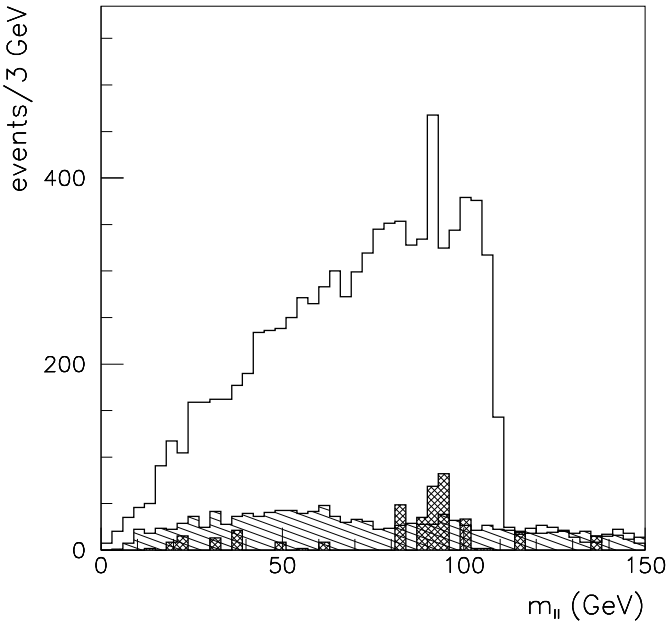

Figure 11: Distributions of invariant mass formed by two OS SF leptons in events passing the selection cuts (see text) for an integrated luminosity of $3 \cdot 10^4$ pb^{-1}. In cross-hatched are SM backgrounds and in hatched the distribution from OS OF leptons.

from 'opposite' sides can be subtracted using opposite flavour (OF) leptons in the same type of events. After this subtraction there are 7433 SUSY events in the plot. The SM backgrounds are shown in cross-hatched and only 385 events are expected. The leptons may come either from the decay $\tilde{\chi}_2^0 \to \ell^+\ell^-\tilde{\chi}_1^0$ or the decay $\tilde{\chi}_2^0 \to \tilde{\ell}\ell$, with the subsequent decays $\tilde{\ell} \to \tilde{\chi}_1^0\ell$. The first decay is a three-body decay, which is strongly suppressed if two-body decays are allowed. Possible two-body decays are $\tilde{\chi}_2^0 \to \mathrm{h}^0\tilde{\chi}_1^0$, $\tilde{\chi}_2^0 \to \mathrm{Z}^0\tilde{\chi}_1^0$ or the already proposed slepton decay. Since the end-point implies a mass difference between the $\tilde{\chi}_2^0$ and $\tilde{\chi}_1^0$ greater than the Z^0 mass, the slepton decay is the most likely candidate. If it is the slepton decay that gives the signal, the position of the edge is a function of the masses of the involved particles according to the expression:

$$m_{\ell\ell}^{\max} = m_{\tilde{\chi}_2^0}\sqrt{1 - \frac{m_{\tilde{\ell}}^2}{m_{\tilde{\chi}_2^0}^2}}\sqrt{1 - \frac{m_{\tilde{\chi}_1^0}^2}{m_{\tilde{\ell}}^2}} \tag{6}$$

For Point 5 the nominal value of this edge is 109 GeV. As shown in the following sections the masses of the involved particles can be measured directly with independent methods and the slepton decay hypothesis can be confirmed. The position of this edge can be measured as $109 \pm 0.30(\text{stat.}) \pm 0.11(\text{syst.})$ GeV.

8 Search for a $\tilde{\chi}_1^0$ Signal

The most distinctive experimental consequence of R-parity violation is the possibility to reconstruct the $\tilde{\chi}_1^0$ mass and thereby constrain the kinematics of the complete SUSY event. For the case of baryonic violating decays of the $\tilde{\chi}_1^0$, six jets need in principle to be identified, measured and combined correctly to form two 3-jet invariant mass combinations. The combinatorial background for taking all jet combinations is considerable, since the number of combinations for pairs of 3-jet combinations among N jets is:

$$\frac{\text{N!}}{3!3!(N-6)!} \tag{7}$$

For events with high jet multiplicities the signal is likely to be drowned in the combinatorial background. For N=6 there are 20 combinations, so even when using the correct 6 jets, a 'clever' selection of combinations would be benificial. By first studying the $\tilde{\chi}_1^0$ decays at the generator level, an indication of the appropriate selection cuts can be found.

8.1 Decays of $\tilde{\chi}_1^0$ at the Generator Level

Since the $\tilde{\chi}_1^0$ comes from decays of heavy particles, the obvious selection criteria are cuts on the angular separation between jets and a hierarchical selection of the p_T of the jets. These quantities have been checked at the generator level. The transverse momentum distributions of the two $\tilde{\chi}_1^0$'s are displayed in figure 12. The harder of the two $\tilde{\chi}_1^0$'s has

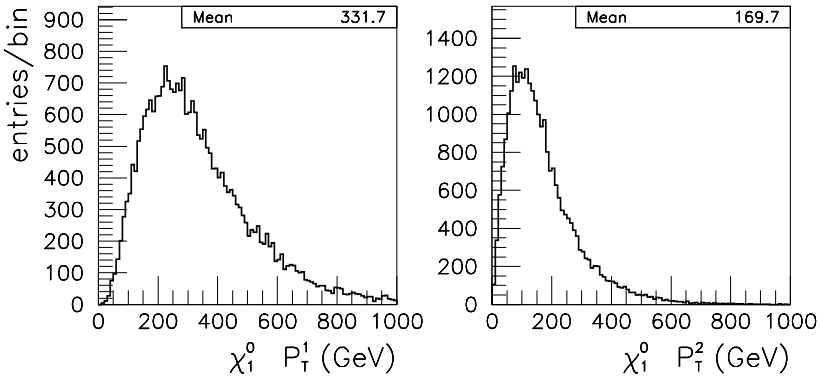

Figure 12: Distribution of the generated transverse momentum for the two $\tilde{\chi}_1^0$'s.

an average p_T of 332 GeV and the softer an average p_T of 170 GeV. The two $\tilde{\chi}_1^0$'s are moreover quite well separated in the detector with an average distance between their four-vectors of ΔR=1.9. In general, the $\tilde{\chi}_1^0$ decays into jets which have p_T's that are close to

the jet acceptance threshold, since it comes last in the SUSY cascade decays of squarks and gluinos. In particular, jets which originate from the *softer* $\tilde{\chi}_1^0$ decay have small p_T compared to the other jets in the event. The p_T of the quarks originating from $\tilde{\chi}_1^0$ decays are shown in figure 13. As one can see, the softest quark has an average p_T of only

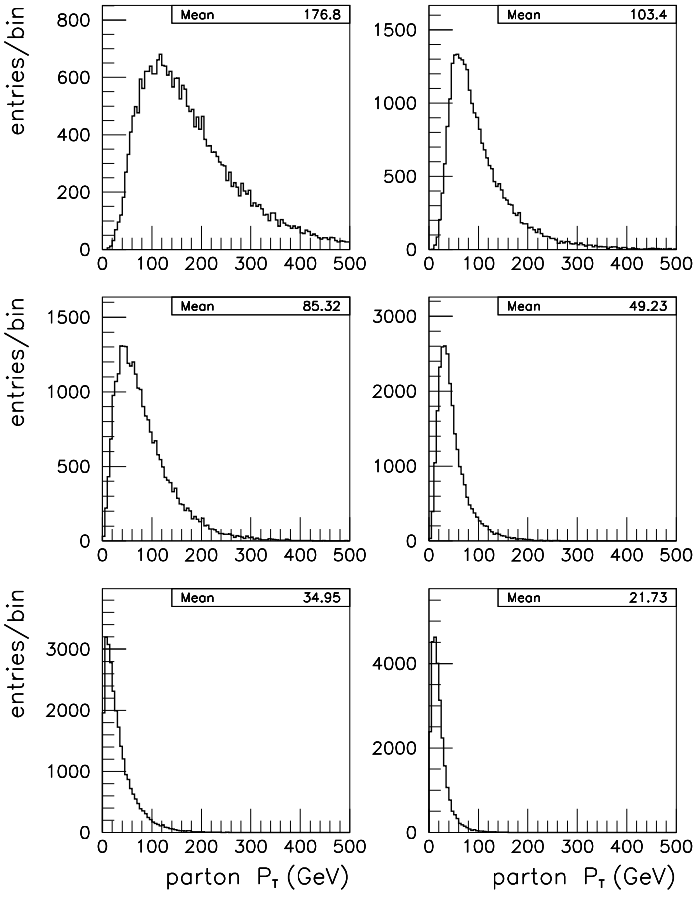

Figure 13: Momentum of quarks from $\tilde{\chi}_1^0$ decays. In the left column the quarks from the harder of the two $\tilde{\chi}_1^0$'s and in the right column from the softer $\tilde{\chi}_1^0$.

21 GeV. Thus, if both $\tilde{\chi}_1^0$'s have to be reconstructed, one must include even very soft jets. Both $\tilde{\chi}_1^0$'s have a considerable boost so the decay products are close together, as shown in figure 14. The average minimum distance between the partons from the harder $\tilde{\chi}_1^0$ decay is only 0.33. The reconstruction efficiency of the $\tilde{\chi}_1^0$ signal varies therefore rapidly with the minimum allowed jet separation and the p_T threshold for the softest jet. The analysis presented in this note relies on reconstructing two 3-jet combinations. Both the p_T and the separation of these jets depend on the mass configuration of the sparticles involved in the production of the $\tilde{\chi}_1^0$'s. It is therefore difficult to give quantitative estimates of how well the reconstruction works for models different from the one considered in this note, but a brief test and a discussion on the generality of this analysis strategy are included in section 10.

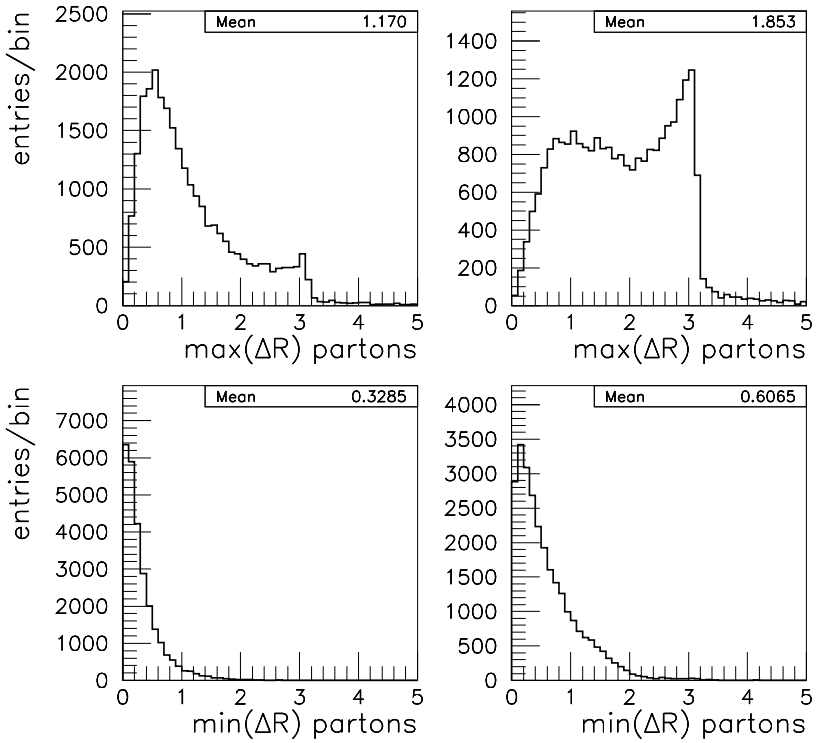

Figure 14: Maximum (top) and minimum (bottom) distance between partons from $\tilde{\chi}_1^0$ decays: the left-hand column correspon to the harder $\tilde{\chi}_1^0$ and the right-hand column to the softer $\tilde{\chi}_1^0$.

8.2 Reconstruction of $\tilde{\chi}_1^0$ Decays

Because of the potentially large combinatorial background discussed above the optimal strategy for reconstructing the $\tilde{\chi}_1^0$ decays is to use events with the smallest possible jet multiplicity which, for the selection cuts used in this analysis, is 8 jets. In principle, $\tilde{q}_R\tilde{q}_L$ production with the decay chains:

$$\begin{array}{rcl} \tilde{q}_R & \rightarrow & \tilde{\chi}_1^0 q \\ & & \hookrightarrow jjj \end{array} \tag{8}$$

and

$$\begin{array}{rcl} \tilde{q}_L & \rightarrow & \tilde{\chi}_2^0 q \\ & & \hookrightarrow \tilde{\ell}\ell \\ & & \hookrightarrow \tilde{\chi}_1^0 \ell \\ & & \hookrightarrow jjj \end{array} \tag{9}$$

results in 8 jets and 2 leptons in the final state. The two hardest jets are likely to come from the squark decays and the 6 other jets from the two $\tilde{\chi}_1^0$'s. Since there are always two $\tilde{\chi}_1^0$'s in each event, the primary production process selected is not crucial for the $\tilde{\chi}_1^0$

reconstruction. The selection cuts are aimed at limiting the combinatorial background, not at selecting explicitly $\tilde{q}_R\tilde{q}_L$ production. Thus, the final event sample may well contain a large fraction of events from $\tilde{g}\tilde{q}$ and $\tilde{q}_L\tilde{q}_L$ production. The event selection criteria are:

- 1 or 2 leptons (e, μ) with $p_T > 20$ GeV
- if two leptons, require them to be OS, SF and $m_{\ell\ell} < 109$ GeV
- at least 8 jets with $p_T > 17.5$ GeV
- veto events with jet 9 $p_T^{jet-9} > 25$ GeV
- two hard jets , $p_T^{jet-1} > 200$ GeV, $p_T^{jet-2} > 100$ GeV, central $|\eta| < 2$ jets
- no b-jet $p_T > 25$ GeV
- $m_{Tcent} > 1000$ GeV
- circularity > 0.2, thrust <0.9

For events that pass this selection, two 3-jet combinations are formed using at least 6 jets, excluding the two leading jets. There is an increase in number of events selected from using additional jets, but this also increases the combinatorial background from other SUSY processes and therefore events with up to 9 jets and a veto for the 9th jet of 25 GeV were chosen. We call these combinations $j^1j^2j^3$ and $j^4j^5j^6$ and form the combinations that pass the following selection:

- p_T of $j^1 > 100$ GeV, p_T of $j^2 < 200$ GeV, p_T of $j^3 < 100$ GeV
- $\Delta R(j^1,j^2) < 1.0$, $\Delta R(j^1+j^2,j^3) < 1.0$
- p_T of $j^4 < 200$ GeV, p_T of $j^5 < 100$ GeV
- $\Delta R(j^4,j^5) < 1.5$, p_T of $j^6 < 50$ GeV
- for j^6 use also jet 9 if $p_T^{jet-9} < 25$ GeV

On average there are 4.6 possible 3-jet combinations in each event for these selection cuts. Combinations are accepted if they fulfill:

- $\Delta m_{jjj} = \min(|m_{j^1j^2j^3} - m_{j^4j^5j^6}|) < 20$ GeV

The resulting m_{jjj} distribution is plotted in figure 15. There is a clear peak centred not far from the $\tilde{\chi}_1^0$ mass of 121 GeV. The plot contains 824 SUSY events for an integrated luminosity of $3 \cdot 10^4$ pb^{-1}, of which 14% come from $\tilde{g}(\to \tilde{q}_R q)\tilde{q}_L$, 10% from $\tilde{g}(\to \tilde{q}_L q)\tilde{q}_R$, 22% from $\tilde{q}_R\tilde{q}_L$, 21% from $\tilde{q}_L\tilde{q}_L$, 14% from $\tilde{g}(\to X)\tilde{q}_L$, 6% from $\tilde{g}(\to X)\tilde{q}_R$ production and 10% from other processes. The distribution is not symmetric, which is partly due to leptons lost inside jets, in which case the reconstructed mass is the one a a slepton (with a nominal mass of 157 GeV). This is apparent when the mass of the $\tilde{\chi}_1^0$ is lowered so the two peaks are resolved (see figure 21). By comparing the reconstructed 3-jet momentum with that of the $\tilde{\chi}_1^0$ partons, it was estimated that 25% of the events have two good reconstructed $\tilde{\chi}_1^0$ and 83% at least one good reconstructed $\tilde{\chi}_1^0$ (ΔR (3-jet momenta,

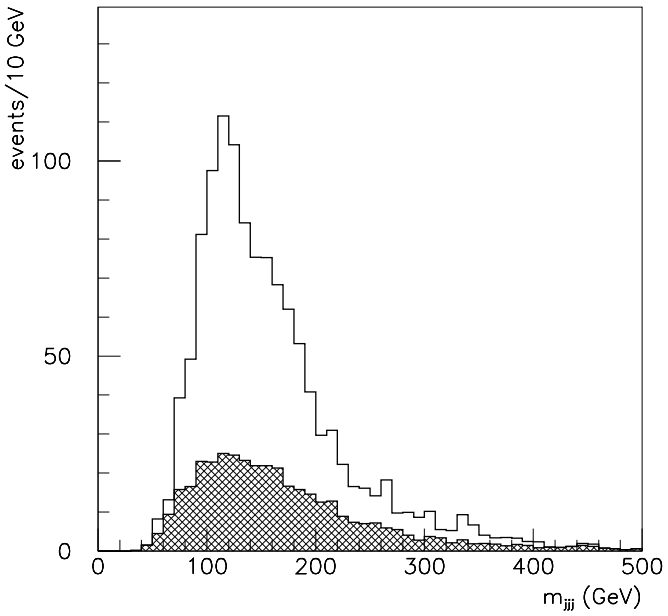

Figure 15: Distribution of the invariant mass of all 3-jet combinations that pass the selection cuts described in the text. The peak corresponding to the $\tilde{\chi}_1^0$ mass is visible. Shown as cross-hatched is the SM backgrounds.

$\tilde{\chi}_1^0$-parton)<0.3). The distribution of invariant mass for tagged events is shown in figure 16. This tagging has some uncertainty, but it gives at least a rough estimate of the reconstruction efficiency. The chosen jet threshold is a trade-off between accepting real signal and rejecting background from initial state radiation. A more detailed study of jet thresholds is presented in the next paragraph.

The SM background, shown as cross-hatched in figure 15, corresponds to 411 events, of which 93% arises from QCD production. The shape of this SM background was modelled using a QCD sample without any requirement on leptons. For the SM background very few events give two 3-jet invariant masses with the selection used. A good cut against QCD background is actually the possibility to form these two 3-jet combinations. The background from SUSY combinatorics and mismeasurements due to overlapping jets is of the same magnitude as the SM background. The influence of the jet veto for the rejection of the QCD background was checked by relaxing the veto threshold for the 9^{th} jet to 30 GeV. With this higher jet veto the QCD background increases by 25%.

The QCD background can be further suppressed by explicitly requiring two leptons in the event:

- 2 leptons (e,μ) with $p_T > 15$ GeV

The resulting 3-jet invariant mass distribution is shown in figure 17. With these cuts 144 events are expected for $3 \cdot 10^4$ pb^{-1}. No generated SM events pass the selection cuts, corresponding to an upper limit at 90% confidence level of 46 QCD events. The peak is Gaussian and the shoulder on the tail at high values of mass is less pronounced. The reconstruction procedure is quite sensitive to the kinematics, since if the $\tilde{\chi}_1^0$ mass is shifted

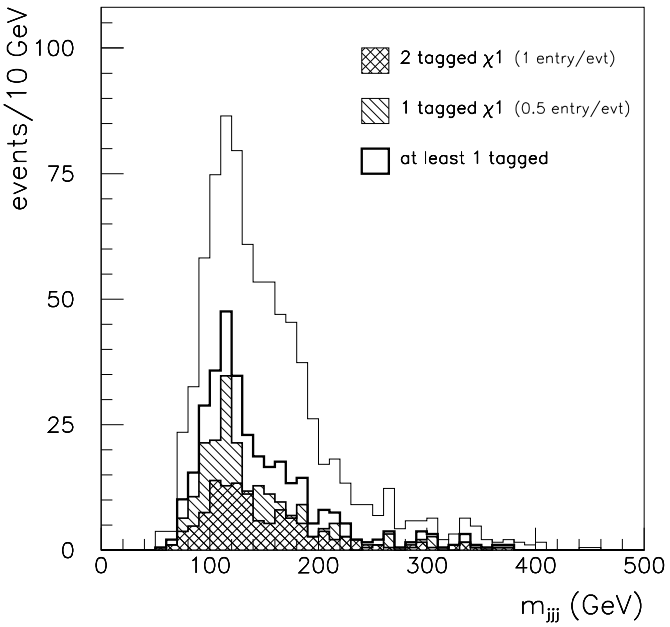

Figure 16: Breakdown of the SUSY signal from figure 15 (normal histogram). The cross-hatched histogram correspons to events with two tagged (see text) reconstructed $\tilde{\chi}_1^0$, the hatched histogram to events with one tagged reconstructed $\tilde{\chi}_1^0$ (0.5 entry/event), and the bold histogram is the sum of the latter two.

down by only 7 GeV the peak in the invariant mass distribution severly degraded. This shows that the jet clustering should be improved and that, to identify 6 jets and obtain a sufficient number of correct combinations, an event sample with higher statistics is needed. Therefore the precision of the $\tilde{\chi}_1^0$ mass measurement is evaluated here assuming that the selection requires only 1 lepton in the final state (see section 8.4).

8.3 Reconstruction of $\tilde{\chi}_1^0$ Using Different Jet Finders

In the previous section it has been shown that the jets from the $\tilde{\chi}_1^0$ are rather soft, close to each other and therefore often overlap. Efficient reconstruction of soft and nearby jets is therefore essential to get a reasonable efficiency for the $\tilde{\chi}_1^0$ reconstruction. Two different jet finders (see section 3.3) have been compared to make sure that the observed reconstructed peak for the $\tilde{\chi}_1^0$ decay does not have a systematic bias due to the chosen jet clustering technique.

The 'mulguisin' jet finder reconstructs 11.7 jets on average and the 'cone' jet finder 11.4 jets for a jet threshold of 17.5 GeV. Figure 18 compares the jet multiplicity distributions obtained with the two jet finders. The 'mulguisin' jet finder is more efficient at separating jets that are closeby or overlapping. Figure 19 compares the $\tilde{\chi}_1^0$ signal obtained for the two different jet finders.

The chosen jet-threshold is a trade-off between accepting real signal and rejecting background from initial state radiation. The jet threshold was varied between 15 and 25 GeV to check its influence. Figure 20 shows the reconstruction efficiencies as a function

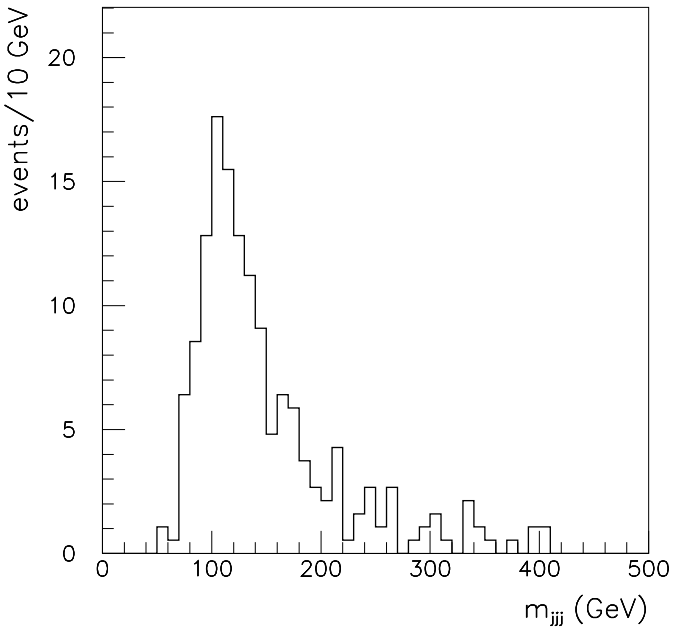

Figure 17: Distribution of the invariant mass of 3-jet combinations for events requiring two leptons for a SUSY sample expected for an integrated luminosity of $3 \cdot 10^4$ pb^{-1}. No generated SM events passed the cuts, corresponding to an upper limit of 46 QCD events at a 90% confidence level.

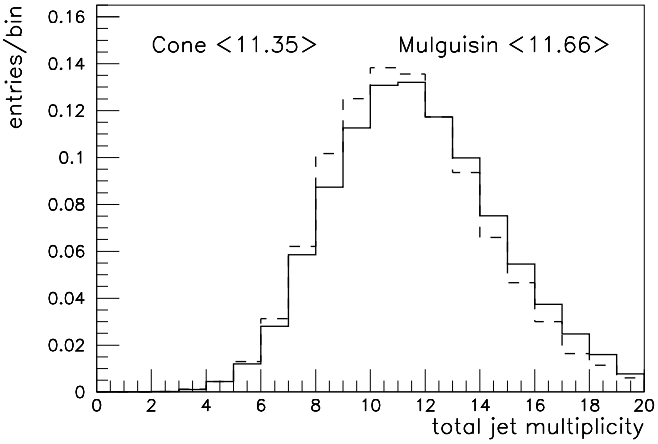

Figure 18: Jet multiplicity obtained for two jet finders.

of the jet threshold. The signal reconstruction works well with both algorithms and the analysis strategy and techniques are independent of the details of the jet clustering. The comparison is not conclusive, although the plots shown here show that the 'cone' algorithm yields more events than 'mulguisin' and indicate that the width of the mass distribution is narrower for 'mulguisin' for all jet thresholds used here. There is no peak in the invariant

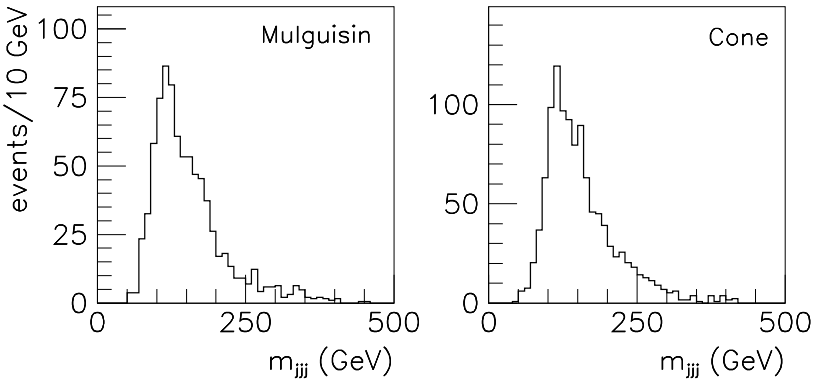

Figure 19: The $\tilde{\chi}_1^0$ reconstructed with the cone and 'mulguisin' jet finder.

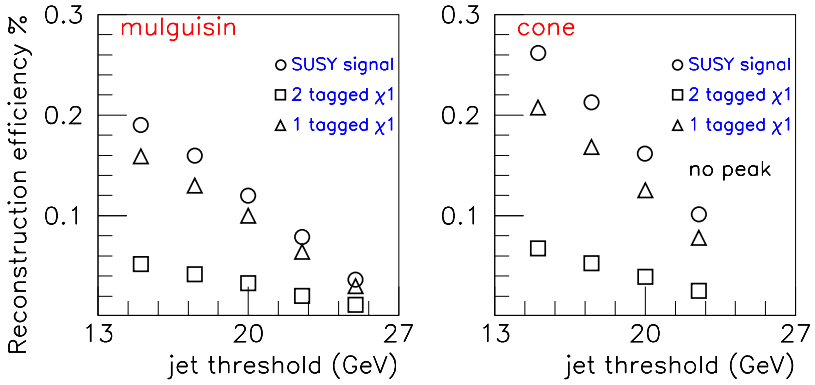

Figure 20: The reconstruction efficiency for $\tilde{\chi}_1^0 \to jjj$ decays as a function of the jet threshold for the 'mulguisin' and 'cone' jet finder.

mass distribution of the 3-jet combinations of the SUSY for a threshold above 20 GeV for the 'cone' algorithm. The 'mulguisin' algorithm is less sensitive to the jet threshold and was therefore chosen for the results presented in this note. It is interesting to note that if a stricter cut, $\Delta m_{jjj} < 10$ GeV, is used the reconstruction efficiency is better for a jet threshold of 17.5 GeV than for 15.0 GeV. The nominal jet threshold used in this analysis is 17.5 GeV. Reconstruction of jets as soft as this should not be a problem during low luminosity operation, but, if for any reason the jet threshold needs to be raised, the quantitative results of this note would be altered accordingly. The loss of signal events can be judged from figure 20. Clearly, a more detailed study, beyond the scope of this work, is need to improve the reconstruction efficiency for $\tilde{\chi}_1^0 \to jjj$ decays. In particular, similarly to the approach used for reconstruction of high p_T $W^{\pm} \to jj$ decays [34, 35], a larger cone can be used to reconstruct the $\tilde{\chi}_1^0$ decay without explicitly require three separate jets to be measured.

8.4 Precision of $\tilde{\chi}_1^0$ Mass Measurement.

The uncertainty of the $\tilde{\chi}_1^0$ mass measurement was evaluated by generating three samples each with a different $\tilde{\chi}_1^0$ mass and with all other masses kept constant at their nominal values. Of course, the kinematics of the events to some extent on the value of the $\tilde{\chi}_1^0$ mass, as shown in table 11. For larger values of the $\tilde{\chi}_1^0$ mass the decay partons carry more

	$m_{\tilde{\chi}_1^0}$ =100 GeV	$m_{\tilde{\chi}_1^0}$ =115 GeV	$m_{\tilde{\chi}_1^0}$ =122 GeV	$m_{\tilde{\chi}_1^0}$ =140 GeV
$< p_T^{\tilde{\chi}_1^0-1} >$	324	330	332	338
$< p_T^{\tilde{\chi}_1^0-2} >$	168	167	170	179
$min(p_T^{quark})$	20.0	20.9	21.7	23.2
$min(\Delta R^{quarks})$	0.288	0.315	0.329	0.352

Table 11: The kinematics at the quarklevel for differents masses of the $\tilde{\chi}_1^0$, with all other masses held nominally at Point 5 values.

momentum and, thus, more jets pass the threshold. For lower of the $\tilde{\chi}_1^0$ mass less energy is released in the $\tilde{\chi}_1^0$ decay and the transverse separations between the jets from the $\tilde{\chi}_1^0$ decay is smaller. These two combined effects cause a degradation of the reconstruction efficiency when the $\tilde{\chi}_1^0$ mass is decreased. The $\tilde{\chi}_1^0$ mass was varied between 115 and 140 GeV whereas all other masses were kept at their nominal value. The invariant mass distributions for three values of the $\tilde{\chi}_1^0$ mass are shown in figure 21. The position of the peak moves as expected. The 'extra' spike around 160 GeV in the top plot is due to unrecognised leptons inside jets from slepton decays, causing the slepton mass to be reconstructed. The peak disappears if it is required that the $jjj-$momentum combined with a lepton should form a slepton. At least for the event sample containing muons, it should be possible to remove this spike by not including in the jet reconstructed non-isolated muons, which fall within the jet cones used for the $\tilde{\chi}_1^0$ reconstruction. The Gaussian fits are to guide the eye and not a measurement of the $\tilde{\chi}_1^0$ mass. The width of the invariant mass distributions are about 22 GeV. The $\tilde{\chi}_1^0$ mass can be measured as $122 \pm 3.1(\text{stat.}) \pm 1.3(\text{syst.})$ GeV.

The sample of top quarks in the all-hadronic decay t $\rightarrow$ Wb with W $\rightarrow jj$ can be used as an in situ calibration of the 3-jet reconstruction. The production cross-section for $t\bar{t}$ is close to 600 pb (800 pb including next-to-leading order contributions) thus yielding large samples of about $2.7 \cdot 10^6$ events/year, with $t\bar{t} \rightarrow$ WbWb $\rightarrow jjbjjb$, and about $1.7 \cdot 10^6$ events/year, with $t\bar{t} \rightarrow$ WbWb $\rightarrow \ell\nu bjjb$. These event samples will allow a thourough study of the systematics of 3-jet reconstruction in events with similar kinematics to the SUSY events. The possibility to reconstruct $t\bar{t}$ in multi-jet events with ATLAS has been demonstrated in [36].

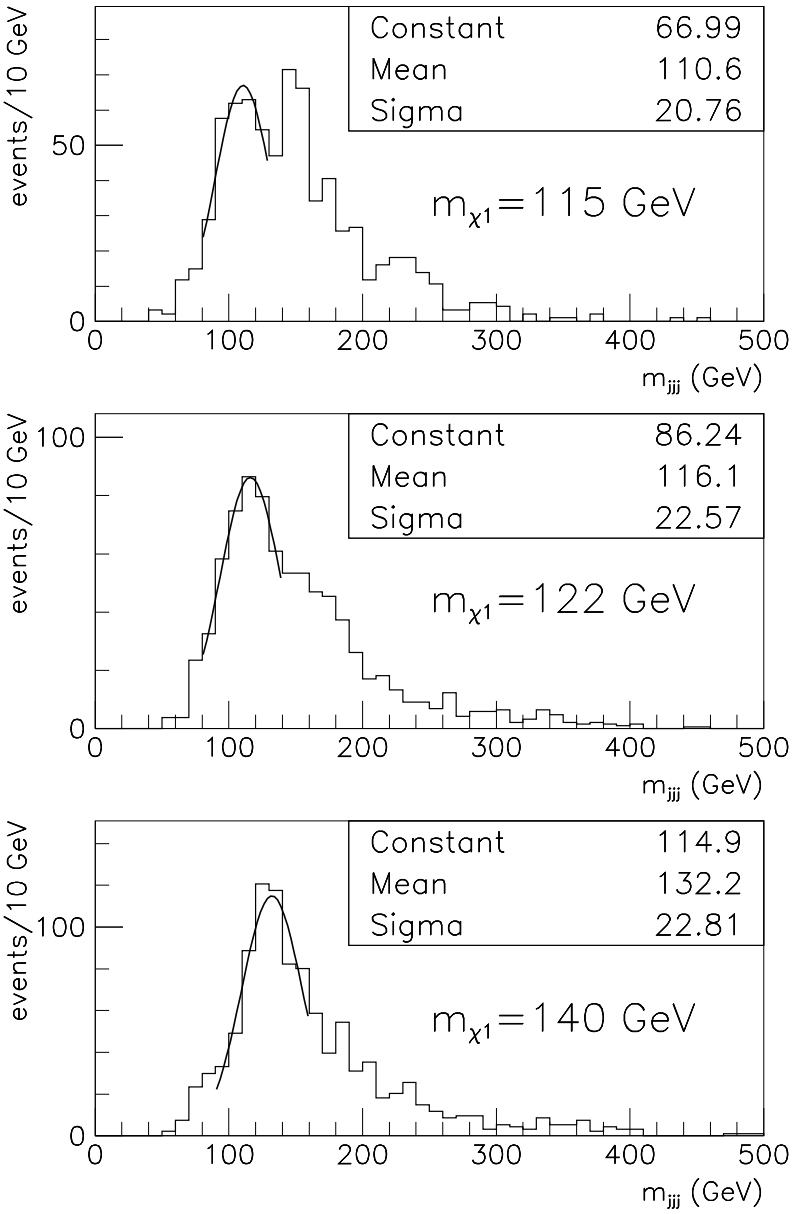

Figure 21: The invariant mass of 3-jet combinations reconstructed for three values of the $\tilde{\chi}_1^0$ mass: $m_{\tilde{\chi}_1^0} = 115$ GeV (top), $m_{\tilde{\chi}_1^0} = 122$ GeV (middle), $m_{\tilde{\chi}_1^0} = 140$ GeV (bottom), for an integrated luminosity of $3 \cdot 10^4$ pb^{-1}. The fits are to guide the eyes only, since the precise measurement of the mass relies on a statistical test where the distributions are compared to a reference Monte Carlo sample.

9 Reconstruction of Other SUSY Particles

Once the $\tilde{\chi}_1^0$'s have been reconstructed and their mass determined, their momenta can be combined with leptons and jets further up the decay chain to reconstruct other sparticle masses. Here it will be demonstrated, without beeing exhaustive, that several sparticles can be directly reconstructed and measured.

9.1 Direct Reconstruction of the $\tilde{\ell}$ and $\tilde{\chi}_2^0$ Masses

The distribution of invariant masses of the OS SF lepton pairs (see section 7) indicated that the observed leptons may come from the decay:

$$\begin{array}{rcl} \tilde{\chi}_2^0 & \rightarrow & \tilde{\ell}_R \ell \\ & & \quad \hookrightarrow \tilde{\chi}_1^0 \ell \\ & & \qquad \hookrightarrow jjj \end{array} \tag{10}$$

If that is the case the slepton mass would be reconstructed when the momenta of the 3 jets from the $\tilde{\chi}_1^0$ are combined with one of the leptons. Events were selected with:

- 2 reconstructed $\tilde{\chi}_1^0$ candidates, $\left| m_{jjj} - m_{\tilde{\chi}_1^0}^{fit} \right| < 30$ GeV
- 2 OS SF leptons with $p_T^{\ell-1} > 15$ GeV , $p_T^{\ell-2} > 10$ GeV and $\mathrm{m}_{\ell\ell} < 109$ GeV

The constraint of the measured $\tilde{\chi}_1^0$ mass is used to recalibrated 3-jet momenta.

A priori, it is not known which $\tilde{\chi}_1^0$ comes from the slepton side. A large fraction of the events have a $\tilde{\mathrm{q}}_R$ that that decays directly to $\tilde{\chi}_1^0 q$ and should therefore give a hard $\tilde{\chi}_1^0$. It is, therefore, assumed that the 3-jet combination with, the smallest p_T comes from the slepton side. Its 3-momentum is combined with that of one of the leptons and the invariant mass of the system is calculated. Due to the mass differences of $\tilde{\chi}_1^0, \tilde{\ell}_R$, and $\tilde{\chi}_2^0$, the softer of the two leptons should come from the slepton decay. However, the efficiency $\tilde{\ell}_R$ efficiency is improved by about 10% if, instead, both leptons are tried and the combination that gives the smaller invariant mass is kept. The resulting invariant mass distribution, which peaks at the expected $\tilde{\ell}_R$ mass of 157 GeV is displayed in figure 22. There are 119 events, including 89 events within $\mathrm{m}_{\ell_R} \pm 20$ GeV, expected for an integrated luminosity of $3 \cdot 10^4$ pb^{-1}.

The $\tilde{\chi}_2^0$ is reconstructed by combining both leptons with the 3-jet momenta of the $\tilde{\chi}_1^0$, after first applying a cut around the $\tilde{\ell}_R$ peak. The invariant mass distribution is shown in figure 23 and a clear peak is visible at the nominal $\tilde{\chi}_2^0$ mass of 233 GeV. The composition of the sample used for the $\tilde{\ell}_R$ and $\tilde{\chi}_2^0$ reconstruction is 30% $\tilde{\mathrm{q}}_R\tilde{\mathrm{q}}_L$, 26% $\tilde{\mathrm{g}}\tilde{\mathrm{q}}_L$, 21% $\tilde{\mathrm{q}}_L\tilde{\mathrm{q}}_L$ and 21% from other processes.

The sensitivity of the reconstruction was checked by first varying the $\tilde{\ell}_R$ mass by ± 10 GeV while keeping all other masses the same. The distributions for two different slepton masses are shown in figure 24. The reconstructed peaks vary as the mass of the slepton. The slepton mass can be measured as $157 \pm 5.1(\mathrm{stat.}) \pm 1.6(\mathrm{syst.})$ GeV. The uncertainty of the $\tilde{\chi}_1^0$ mass used for the $\tilde{\chi}_1^0$ mass constraint of the 3-jet momenta is included in the statistical error. The $\tilde{\chi}_2^0$ mass was varied by ± 20 GeV and the corresponding mass distributions are shown in figure 25 for the three choices of the $\tilde{\chi}_2^0$ masses. The $\tilde{\chi}_2^0$ mass can be measured as $233 \pm 4.1(\mathrm{stat.}) \pm 2.3(\mathrm{syst.})$ GeV.

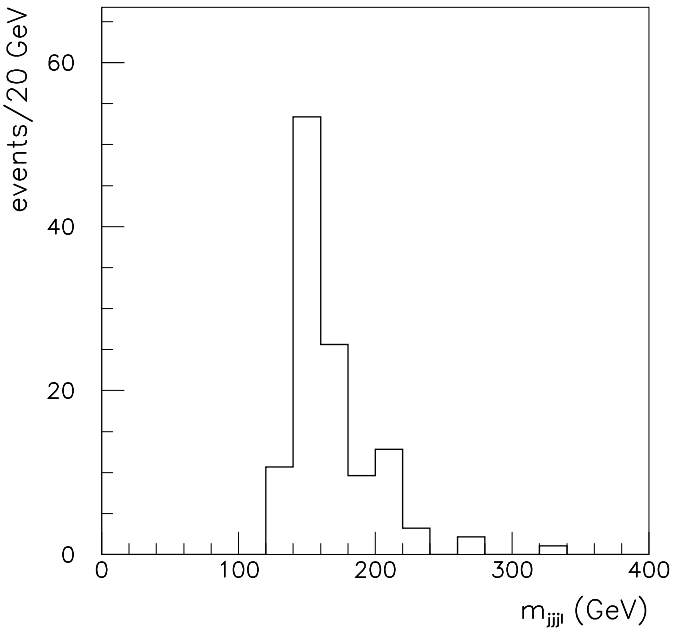

Figure 22: Distribution of the smaller of the invariant masses of the softer $\tilde{\chi}_1^0$ candidate combined with one of the two leptons. A clear peak around the $\tilde{\ell}_R$ ($\tilde{\ell}_R = \tilde{e}, \tilde{\mu}$) mass of 157 GeV is visible. No SM backgrounds pass the selection cuts.

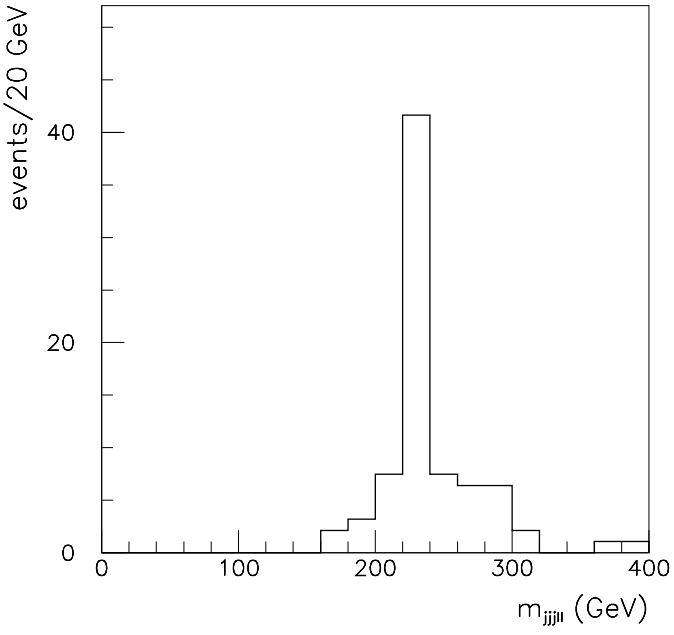

Figure 23: Invariant mass distribution of the softer $\tilde{\chi}_1^0$ candidates combined with two leptons. A clear peak at the expected $\tilde{\chi}_2^0$ mass is visible. No SM backgrounds pass the selection cuts.

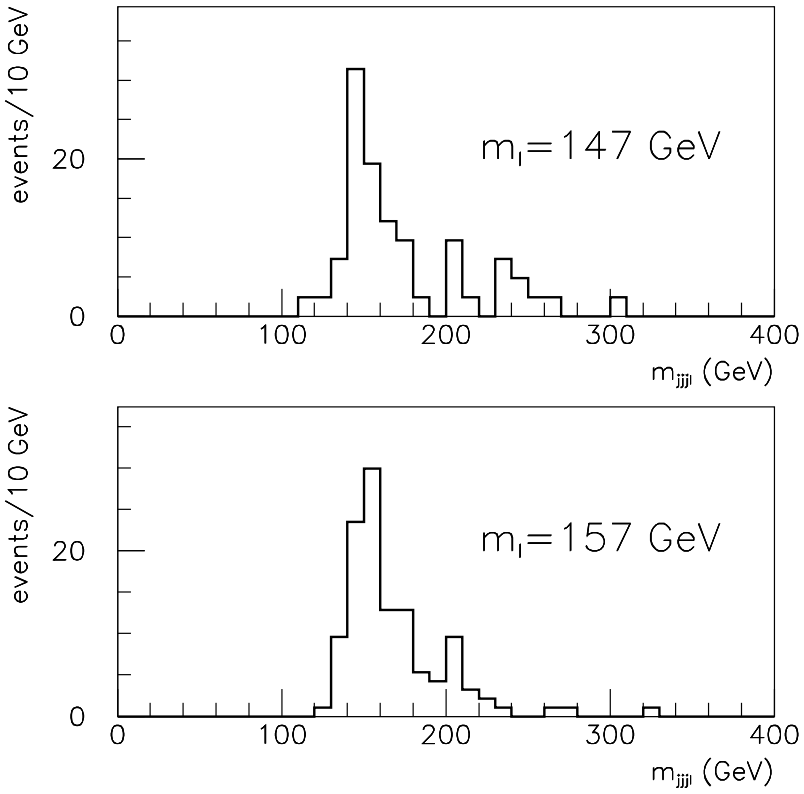

Figure 24: Distribution of the $m_{jjj\ell}$ invariant mass for two values of the $\tilde{\ell}_R$ mass, $m_{\tilde{\ell}_R}$=147 GeV (top), $m_{\tilde{\ell}_R}$=157 GeV (bottom).

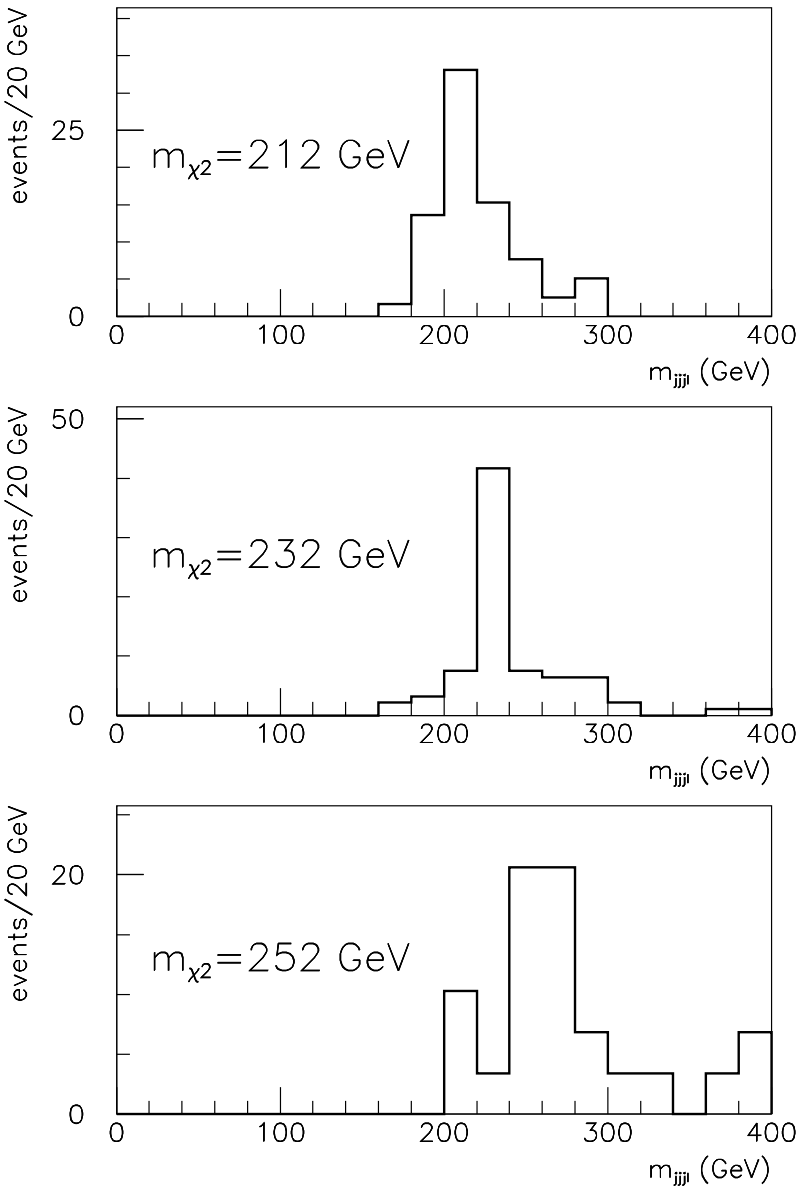

Figure 25: Distribution of the $m_{jjj\ell}$ invariant mass for three values of the $\tilde{\chi}_2^0$ mass, $m_{\tilde{\chi}_2^0}$=212 GeV (top), $m_{\tilde{\chi}_2^0}$=232 GeV (middle) and $m_{\tilde{\chi}_2^0}$=252 GeV (bottom).

9.2 Reconstruction of Squarks Masses

With both gaugino ($\tilde{\chi}_1^0, \tilde{\chi}_2^0$) and scalar ($\tilde{\ell}_R$) masses measured, one can now try to reconstruct heavier particles further up the decay chain. The cuts used for the $\tilde{\chi}_1^0$, $\tilde{\ell}$ and $\tilde{\chi}_2^0$ reconstruction are loosely aimed at selecting $\tilde{\mathrm{q}}_R\tilde{\mathrm{q}}_L$ primary production. One can now try to combine the *harder* of the $\tilde{\chi}_1^0$ candidates with a hard jet with the aim of reconstructing the decay:

$$\begin{array}{rcl} \tilde{\mathrm{q}}_R & \rightarrow & \tilde{\chi}_1^0 q \\ & & \quad \hookrightarrow jjj \end{array} \tag{11}$$

One can also try to reconstruct a distribution sensitive to the $\tilde{\mathrm{q}}_L$ mass by combining the *softest* $\tilde{\chi}_1^0$ candidate with a hard jet from the decay:

$$\begin{array}{rcl} \tilde{\mathrm{q}}_L & \rightarrow & \tilde{\chi}_2^0 q \\ & & \quad \hookrightarrow \tilde{\ell}\ell \\ & & \qquad \hookrightarrow \tilde{\chi}_1^0 \ell \end{array} \tag{12}$$

Due to the low statistics of fully reconstructed $\tilde{\chi}_2^0$, it is not possible for an integrated luminosity of $3 \cdot 10^4$ pb^{-1} to reconstruct the complete $\tilde{\mathrm{q}}_L$ decay chain above. Events are selected with the following cuts:

- 2 reconstructed $\tilde{\chi}_1^0$ candidates, $\left| m_{jjj} - m_{jjj}^{fit} \right| < 30$ GeV
- two hard central jets with $|\eta| < 2$, $p_T^1 > 300$ GeV and $p_T^2 > 100$ GeV

The selected events are from the combined production of 11% $\tilde{\mathrm{g}}(\rightarrow \tilde{\mathrm{q}}_L q)\tilde{\mathrm{q}}_R$, 11% $\tilde{\mathrm{g}}(\rightarrow \tilde{\mathrm{q}}_R q)\tilde{\mathrm{q}}_L$, 28% $\tilde{\mathrm{q}}_R\tilde{\mathrm{q}}_L$, 21% $\tilde{\mathrm{q}}_L\tilde{\mathrm{q}}_L$, and 29% from other processes. In total, 50% of the events contain a $\tilde{\mathrm{q}}_R$, which comes either from direct production or from a gluino decay. It is not known a priori which of the hard jets comes from the $\tilde{\mathrm{q}}_R$-decay. Therefore, both jets are first combined with the *soft* $\tilde{\chi}_1^0$ candidate and the lepton(s). The combination that gives the smallest mass is retained. The other hard jet is then combined with the *hard* $\tilde{\chi}_1^0$ candidate and the resulting distribution for the invariant mass is shown in figure 26. This distribution displays a broad peak around 660 GeV, which is in rough agreement with the $\tilde{\mathrm{q}}_R$ mass. The mass distribution for events containing a $\tilde{\mathrm{q}}_R$ from direct production or from a gluino decay is indicated as a bold histogram. The distribution contains 209 events, of which 83% are within $\mathrm{m}_{\tilde{\mathrm{q}}_R} \pm 100$ GeV, for an integrated luminosity of $3 \cdot 10^4$ pb^{-1}. The mass distributions obtained with the *soft* $\tilde{\chi}_1^0$ is compared to that of figure 26 in figure 27, where one can see that the edge of the former distribution corresponds to the peak of the latter. This gives confidence in the procedure since the latter case reconstructs all decay products and forms the $\tilde{\mathrm{q}}_R$ mass, whereas for the case of the *soft* $\tilde{\chi}_1^0$ not all decay products are reconstructed so the distribution is wider and has an edge structure. To verify that the distribution in figure 26 is actually a measurement of the $\tilde{\mathrm{q}}_R$ mass and not a mixture of squarks, the $\tilde{\mathrm{q}}_L$ mass was decreased by 100 GeV. The resulting distribution is shown in the middle plot of figure 28 and one can see that the peak stays in the same position and that the shape of the distribution is only marginally affected. If, instead, the $\tilde{\mathrm{q}}_R$ mass is decreased by 100 GeV, the peak is displaced accordingly, as can be seen

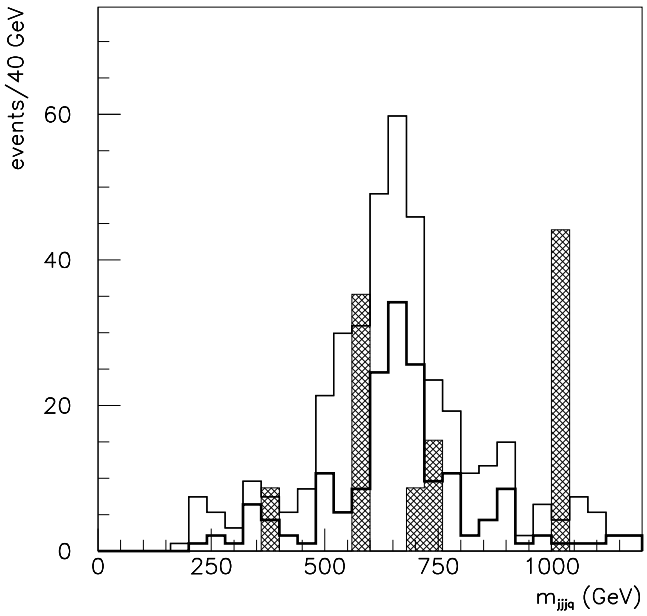

Figure 26: Invariant mass distribution obtained by combining the *hard* $\tilde{\chi}_1^0$ candidate with one of the hard jets in the event. A broad but clear peak around the squark mass of 667 GeV is visible. The bold histogram corresponds to events coontaining a $\tilde{q}_R$. The cross-hatched histogram represents the residual SM background.

in the bottom plot of figure 28. Even if only 50% of the selected events contain a $\tilde{q}_R$, the peak of figure 28 does provide a measurement of the $\tilde{q}_R$ mass, which can be measured to $664 \pm 30(\text{stat.}) \pm 7(\text{syst.})$ GeV. Measurements at high luminosity will be needed to improve the measurement of the $\tilde{q}_R$ mass and possibly to also extract the $\tilde{q}_L$ mass using events containing two leptons and 8 jets.

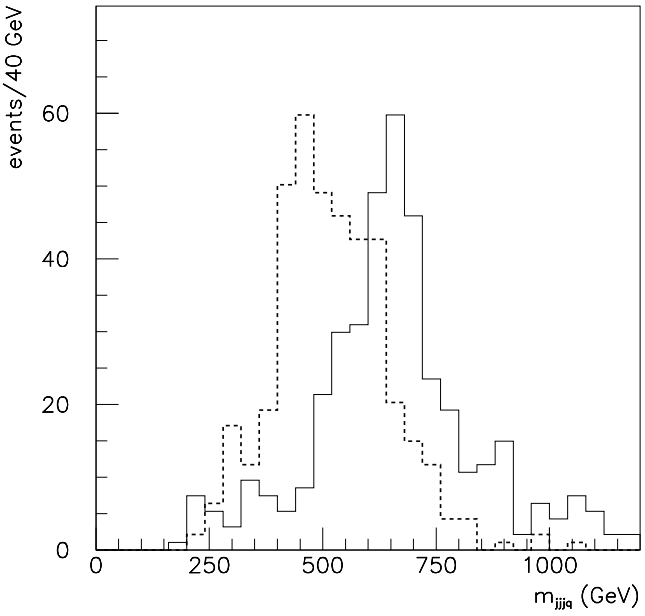

Figure 27: Invariant mass distributions of the two $\tilde{\chi}_1^0$ candidates combined with the two hardest jets (see text).

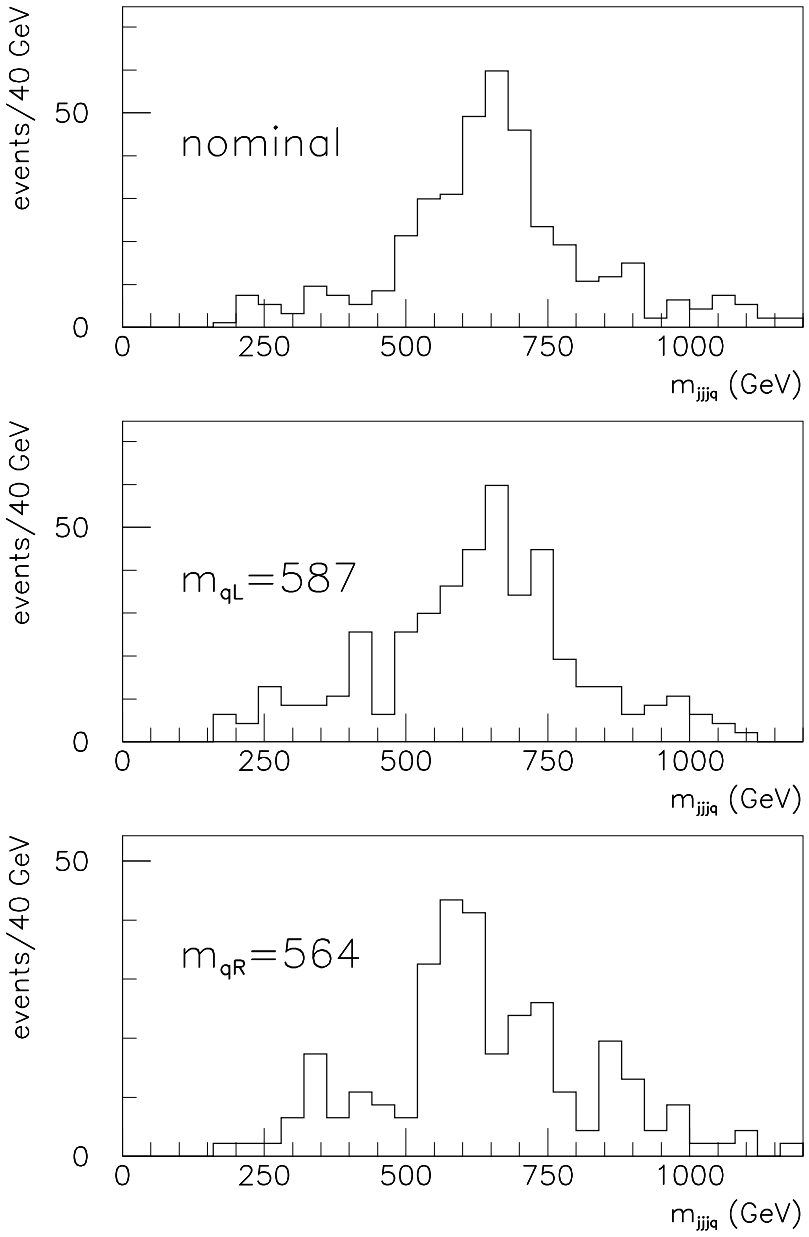

Figure 28: The *hard* $\tilde{\chi}_1^0$ candidate combined with the hard jet. Top plot: The distribution for the nominal squark masses. Middle plot: The $\tilde{q}_L$ mass is lowered by 100 to 587 GeV. Bottom plot: The $\tilde{q}_R$ mass is lowered by 100 to 564 GeV. The position of the peak shows that the distribution is sensitive to the $\tilde{q}_R$ mass and is only weakly sensitive to the $\tilde{q}_L$ mass.

9.3 Search for the Light Higgs Boson.

In the SUSY scenario where R-parity was conserved, the reconstruction of the light Higgs boson through its dominant decay mode $h^0 \to b\bar{b}$ was straightforward and gave a robust signal [6, 8]. The SM backgrounds are, in the R-parity conserved scenario, suppressed by a cut on missing transverse energy, which of course cannot be applied here. The suppression of SM background when R-parity is violated relies on requiring at least one lepton and/or the reconstruction of two $\tilde{\chi}_1^0$ decays. A combined requirement of a lepton and 2 b-jets would reduce the event sample so much that no measurement of the h^0 mass would be possible. Therefore, events are selected with the following cuts:

- at least 8 jets with $p_T > 17.5$ GeV
- no additional jet with p_T 25 GeV (not tagged as b-jet)
- two hard central jets with $|\eta| < 2$, $p_T^{jet1} > 200$ GeV and $p_T^{jet2} > 100$ GeV
- 2 tagged b-jets with p_T^{b} >30 GeV
- no additional b-jet with p_T >25 GeV
- $m_{Tcent} > 1000$ GeV

For the selected events, the $\tilde{\chi}_1^0$ mass was reconstructed using the same requirements for forming 3-jet invariant masses as in section 8.2. Events with:

- 2 reconstructed $\tilde{\chi}_1^0$ candidates, with $\left| m_{jjj} - m_{\tilde{\chi}_1^0}^{fit} \right| < 30$ GeV
- ΔR^{bb} <2.0

were kept and the invariant mass of the 2 b-jets was calculated.

To check that the $h^0 \to b\bar{b}$ signal can be actually reconstructed in this case, a perfect 100% tagging of b-jets and perfect rejection of other jets is first assumed. The obtained distribution is shown as an inset in figure 29. A clear peak is seen above the combinatorial background, which, however, is larger than in the case where R-parity is conserved [6]. Using the nominal expected b-tagging performance the combinatorial background increases substantially and together with the QCD background the $h^0 \to b\bar{b}$ signal becomes marginal as shown in figure 29. There is a very large uncertainty on the QCD background in this plot due to the limited residual statistics in the Monte Carlo sample. The histogram shown originates from only a few events and its shape was invented just to illustrate the poor signal-to-background ratio. In figure 30, the $h^0 \to b\bar{b}$ distribution is plotted as reconstructed with the 'cone' jet finder. The SUSY background is also large due to the misidentification of c-jets originating from the $\tilde{\chi}_1^0$ decays. The result is basically independent of the jet finder and the conclusion is that it will be extremely difficult at low luminosity to use the $h^0 \to b\bar{b}$ channel in SUSY events to discover the h^0 boson and measure its mass. The h^0 boson mass would in any case be best measured in the $h^0 \to \gamma\gamma$ channel, which will only be possible at high luminosity. With 10^5 pb^{-1} of data collected, it is possible to measure the h^0 boson mass with a total precision of 0.3 GeV, improving ultimately to 0.2 GeV for $3 \cdot 10^5$ pb^{-1} of collected statistics [36].

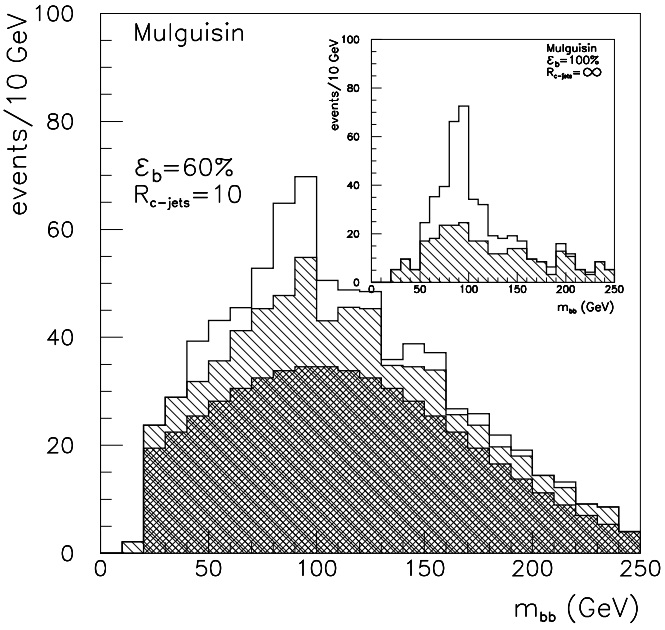

Figure 29: Reconstructed $b\bar{b}$ invariant mass for $\not{R}$ SUSY events, selected as described in the text, using the 'mulguisin' jet finder. The SUSY combinatorial background is shown as hatched histogram and the SM background as cross-hatched. The inset shows the SUSY signal assuming 100% b-tagging efficiency and perfect rejection of non-b-jets.

The rate of observed b-jets is enhanced by the production of h^0 bosons in SUSY cascade decays through the decay $h^0 \to b\bar{b}$. Even if the $b\bar{b}$-peak could not be used for a measurement of the mass of the h^0 boson, the rate of b-jets in SUSY events may indicate the presence of $h^0 \to b\bar{b}$ decays. The dominant production of h^0 is from the decays $\tilde{\chi}_2^0 \to \tilde{\chi}_1^0 h^0$ and this rate depends on the mass of the h^0 and its couplings, which are functions of the SUGRA parameters μ and $\tan\beta$. In figure 31 the branching fraction for $\tilde{\chi}_2^0 \to \tilde{\chi}_1^0 h^0$ is shown as a function of these parameters. It can be seen that for negative μ and $\tan\beta$ larger than 4 h^0 production is strongly suppressed, and that the observed b-jet rate may be used to constrain the sign of μ.

9.4 Sensitivity to the Gluino Mass

In section 6.3 it was shown that there is a sizeable rate of events with multiple b-jets. It has already been shown in previous studies that the ratio of events with 2 b-jets to those with 4 b-jets could be used to estimate the gluino mass [3]. Since it is here difficult to isolate the $h^0 \to b\bar{b}$ signal due to the much higher jet multiplicity and the large number of c-jets the rate of events with 2 b-jet cannot be measured reliably. The events with 4 b-jets, however, have a very good signal-to-background ratio. The final states with 4 b-jets are dominated by $\tilde{g}\tilde{g}$, $\tilde{g}\tilde{q}$ production, where the gluino decays to heavy flavour squarks:

- $(X+)\tilde{g} \to \tilde{t}_1 t \to t\bar{t}\tilde{\chi}_2^0 \to WbWb(h^0 \to b\bar{b})\tilde{\chi}_1^0\tilde{\chi}_1^0(+X')$
- $\tilde{g}\tilde{g} \to \tilde{t}_1 t\bar{t}_1 t \to t\bar{t}t\bar{t}\tilde{\chi}_1^0\tilde{\chi}_1^0 \to WbWbWbWb\tilde{\chi}_1^0\tilde{\chi}_1^0$

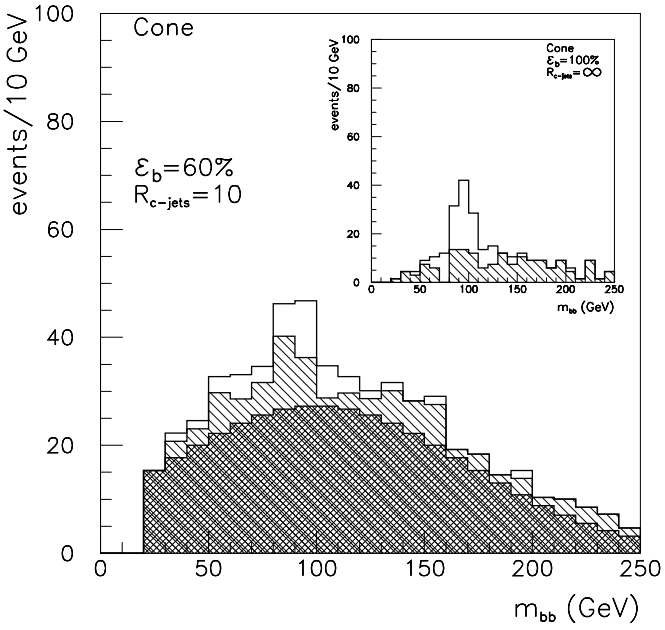

Figure 30: Reconstructed $b\bar{b}$ invariant mass for $\not{R}$ SUSY events, selected as described in the text, using the 'cone' jet finder. The SUSY combinatorial background is shown as hatched histogram and the SM background as cross-hatched. The inset shows the SUSY signal assuming 100% b-tagging efficiency and perfect rejection of non-b-jets.

- $\tilde{g}\tilde{q}_L \to \tilde{q}_L\tilde{q}_L q \to \tilde{\chi}_2^0\tilde{\chi}_2^0 qq \to qq\tilde{\chi}_1^0\tilde{\chi}_1^0(h^0 \to b\bar{b})(h^0 \to b\bar{b})$

with the additional channels where the stop quark is replaced by a sbottom. A lighter gluino would result in enhanceed production cross-sections for $\tilde{g}\tilde{g}$ and $\tilde{g}\tilde{q}$ and a heavier gluino in reduced prodiction cross-sections production. The rate of events with four (and more) b-jets can be measured in a sample obtained by requiring:

- at least 8 jets with $p_T > 25$ GeV
- $m_{Tcent} > 1000$ GeV
- circularity> 0.2 and thrust< 0.9
- at least 1 lepton ($e\mu$) with $p_T > 10$ GeV
- at least 4 b-jets with $p_T > 50$ GeV

No SM background events pass these selection cuts. The production cross-sections for different SUSY processes are given in table 12 for three different masses of the gluino (the squark masses were kept at their nominal values). As the mass of the gluino decreases, the rate of four b-jets increases. As compared to Point 1, with R-parity conserved, the ratio of events with 2 b-jets to those with 4 b-jets cannot be used and, instead, the measurement presented here relies on the determination of an absolute rate which will be dominated by systematic uncertainties. However, the measurement of the rate of events with 4 b-jets

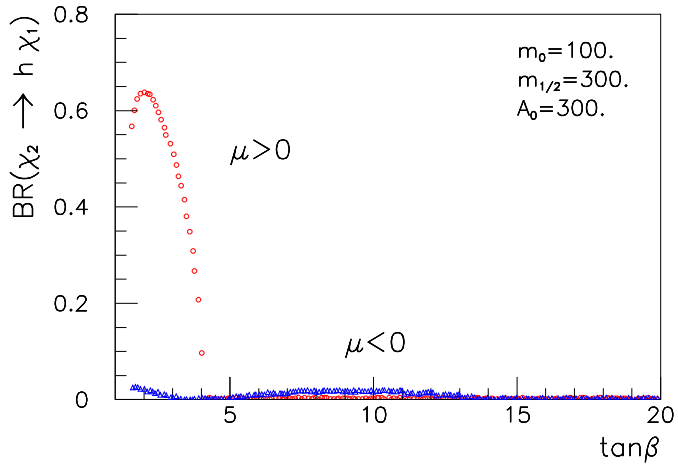

Figure 31: Branching ratio for the decay $\tilde{\chi}_2^0 \to \tilde{\chi}_1^0 h^0$ as a function of tanβ for each sign of μ for fixed values of the other SUGRA parameters.

$m_{\tilde{g}}$	σ_{tot}	$\sigma_{\tilde{g}\tilde{g}'\tilde{g}\tilde{q}}$	$N_{4b(tot)}$	$N_{4b(\tilde{g}\tilde{g})}$	$N_{4b(\tilde{g}\tilde{q})}$	$N_{4b(\tilde{q}\tilde{q})}$
700	22.15 pb	13.33 pb	443	257	124	9
768	17.78 pb	9.28 pb	256	107	96	0
840	14.48 pb	6.50 pb	168	81	58	0

Table 12: Expected cross-sections and rates for events with at least four tagged b-jets as a function of the gluino mass for different SUSY production processes for an integrated luminosity of $3 \cdot 10^4$ pb^{-1}.

can provide some sensitivity to the gluino mass and serve as a cross-check of the gluino mass possibly obtained by other measurements, e.g. in the stop sector, or predicted by fits to a model constrained by other measurements.

10 Reconstruction of $\tilde{\chi}_1^0$ for Other Models

The reconstruction of the $\tilde{\chi}_1^0$ in Point 5 has been demonstrated in the case of baryonic R-parity violation. An important question is whether SUSY particles can still be observed and measured in a large part of the parameter space if R-parity is violated and the $\tilde{\chi}_1^0$'s give hadronic final states. The rejection of SM backgrounds relied on selecting events with multiple jets and requiring at least one lepton. Fortunately, leptons are frequently produced in SUSY decays. Figure 32 shows the cross-section times branching ratio for at least one lepton produced in SUSY decays, mapped over the $m_0 - m_{1/2}$ plane for tanβ =2.0 and μ >0. It appears that the lepton requirement can be generally applied. Another efficient cut against SM background is the reconstruction of two $\tilde{\chi}_1^0$ candidates. Very few QCD events pass this cut. However, the direct reconstruction depends on the details of the kinematics and it is therefore difficult to give a quantitative estimate without doing the

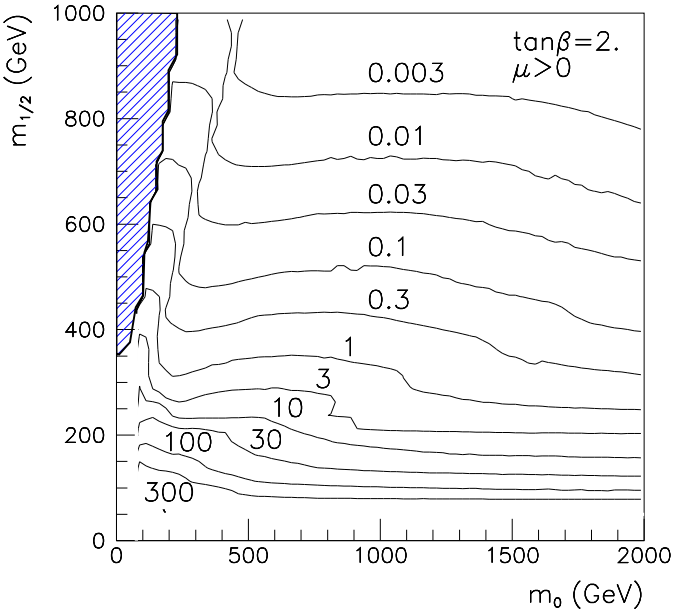

Figure 32: A contour plot of cross-sections×branching ratio in pb in the $m_0 - m_{1/2}$-plane for events with at least 1 lepton produced in SUSY cascade decays for $\tan\beta = 2$ and $\mu > 0$. The upper hatched region is excluded by theory. (Parts of this region may, however, be allowed with R-parity violated, since it is mainly excluded because the $\tilde{\chi}_1^0$ is not the LSP which it does not have to be in $\not{R}$ models.)

simulation and full analysis, which is beyond the scope of this work. If the $\tilde{\chi}_1^0$ is successfully reconstructed it is likely that at least a few other sparticles can be measured. The heavy sparticles are difficult to measure due to the large SUSY combinatorial background. It is difficult to select pure $\tilde{q}_R$ event samples, which reduce combinatorics since $\tilde{q}_R$ always decays directly to $\tilde{\chi}_1^0$ through $\tilde{q}_R \to \tilde{\chi}_1^0 q$. For Point 5 it was, however, demonstrated that a purity of about 50% could be obtained, so that a measurement of the $\tilde{q}_R$ mass was possible. In this section, the discussion is limited to the reconstruction of the $\tilde{\chi}_1^0$ for models previously studied with R-parity conserved, namely Points 1-4.

10.1 Point 1 and Point 2

Point 1 and Point 2 have the same SUGRA parameters except for $\tan\beta$ which is 2 and 10, respectively. Point 2 has been considered here. The masses of interest for the reconstruction of $\tilde{\chi}_1^0$ are given in table 13. The total cross-section is 3.3 pb, of which 0.43 pb are for $\tilde{q}_R\tilde{q}_L$ and 1.36 pb for $\tilde{g}\tilde{q}$ production. At Point 2 the $\tilde{q}_L$ has a 60% branching ratio to decay as $\tilde{q}_L \to \tilde{\chi}_1^{\pm} q$. The chargino subsequently decays with 99% probability as $\tilde{\chi}_1^{\pm} \to \tilde{\chi}_1^0 W^{\pm}$. The leptonic decay of the $W^{\pm}$ gives a hard lepton that can be used for triggering. This gives the same final state as for Point 5. An identical approach for the $\tilde{\chi}_1^0$ reconstruction can therefore be used, but with some adjustments of the cut values due to the heavier sparticles. The resulting m_{jjj} distribution is plotted in figure 33. There are 280 reconstructed SUSY events for an integrated luminosity of $3 \cdot 10^4$ pb^{-1}, that give

Sparticle	Mass (GeV)	Sparticle	Mass (GeV)
$\tilde{q}$	950	$\tilde{g}$	1008
$\tilde{\chi}_1^0$	168	$\tilde{\chi}_1^{\pm}$	322

Table 13: Some sparticle masses for SUGRA Point 2 using `ISAJET` (version 7.31).

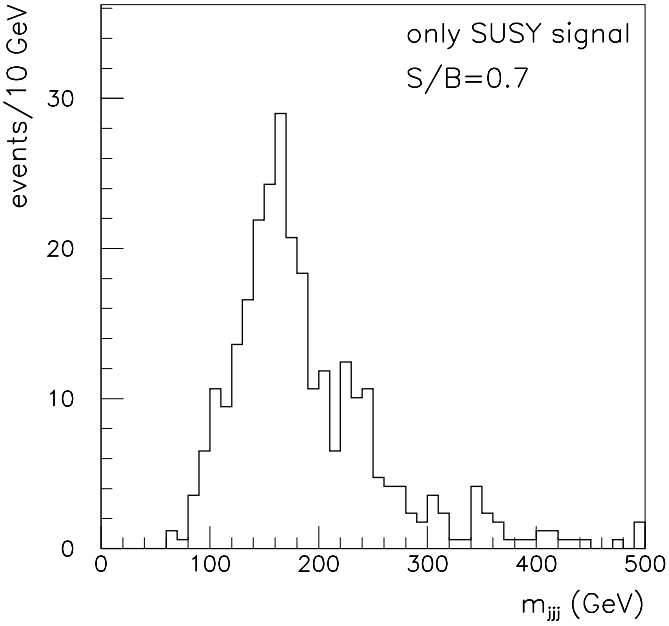

Figure 33: Distribution of the invariant mass of two 3-jet combinations that pass the selection described in the text. The SM background amounts to 395 events, which are not shown here.

a clear peak at the expected $\tilde{\chi}_1^0$ mass of 168 GeV. There are 395 QCD events that pass the selection resulting in a signal-to-noise ratio of 0.7. One should therefore improve the SM background rejection further to establish a convincing signal. Due to statistical fluctuations in the limited QCD Monte Carlo sample, only the SUSY signal is shown in figure 33. The events in the plot can be divided into 13% $\tilde{g}(\rightarrow \tilde{q}_R q)\tilde{q}_L$, 4% $\tilde{g}(\rightarrow \tilde{q}_L q)\tilde{q}_R$, 30% $\tilde{q}_R\tilde{q}_L$, 22% $\tilde{q}_L\tilde{q}_L$, production and 31% from other processes. The sensitivity to the $\tilde{\chi}_1^0$ mass was checked by changing its mass to 130 and 200 GeV, as shown in figure 34. No attempt has been made to measure any other sparticles nor tailor the cuts to optimize the reconstruction for this specific model. It is encouraging that the same technique used for Point 5 also worked for this model, despite the fact that the cross-section is almost ten times smaller. The reconstruction efficiency increases rapidly when the mass of the $\tilde{\chi}_1^0$ increases so the total number of reconstructed events decreases much slower than the cross-section. Most likely, with a more detailed study, the signal reconstruction efficiency and background rejection can be improved.

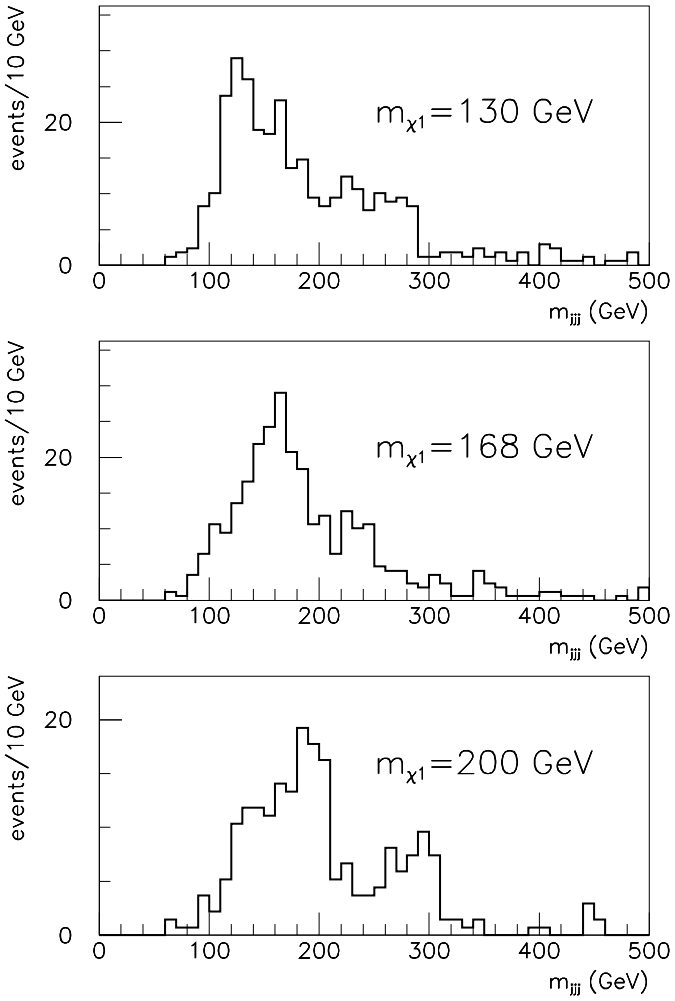

Figure 34: Distributions of 3-jet invariant mass reconstructed for Point 2 for three values of the $\tilde{\chi}_1^0$ mass, 130 GeV (top), 168 GeV (middle) and 200 GeV (bottom). Only the SUSY signal is shown.

10.2 Point 3

Point 3 is the model studied that have the smallest sparticle masses. Therefore the cross-section is very large greater than 1 nb. The light Higgs boson has a mass of only 68 GeV and thus this model is almost ruled out by the most recent LEP2 limits of 64.5 GeV [37][h], but it is still worthwhile to consider the consequences for detection of sparticles in case of R-parity violation. Since the decay $\tilde{\chi}_2^0 \to \tilde{\chi}_1^0 \mathrm{h}^0(\mathrm{Z}^0)$ is kinematically not allowed, the three body decay $\tilde{\chi}_2^0 \to \tilde{\chi}_1^0 \ell^+ \ell^-$ has a branching ratio of 17% per lepton flavour. This gives rise to many events with 2 and 4 isolated leptons. The 4 lepton signature has a very small SM background. Furthermore, in the previous study with R-parity conserved the analysis for Point 3 did not use the cut on missing transverse energy, so it is clear that this model would easily be detected even if R-parity is violated [4, 8]. The dilepton pairs

[h] It is not clear what the implication of R-parity violation is on this limit.

provide a very accurate measurement of the mass difference between $\tilde{\chi}_2^0$ and $\tilde{\chi}_1^0$ that will help to constrain at least the SUGRA parameter $m_{1/2}$ [4, 8, 38]. In SUGRA models, the GUT relations of the gaugino masses give $m_{\tilde{\chi}_2^0} \approx 2 \cdot m_{\tilde{\chi}_1^0} \approx 0.8 \cdot m_{1/2}$. It was also shown that partial reconstruction determines the $\tilde{\chi}_2^0$ momenta if the $\tilde{\chi}_1^0$ mass was assumed. The $\tilde{\chi}_1^0$ has a mass of only 44 GeV and decays to very soft jets. Another strategy than the one reconstructing two $\tilde{\chi}_1^0$ from six jets need therefore to be developed. For the kinematics of a low mass $\tilde{\chi}_1^0$ decay and its reconstruction is limited to Point 4 discussed below.

Most of the measurements except possibly the ones relying on a hard b-jet vetoes, examined in the study with R-parity conserved will still be possible also if R-parity is violated. These measurements will also constrain the global SUGRA parameters even in the case of R-parity violation.

10.3 Point 4

Point 4 also has a relatively light $\tilde{\chi}_1^0$ with a mass of 80 GeV. The phenomenology of Point 4 differs from the other models since it has a large value of m_0, which results in squarks substantially heavier than the gluino. The dominant production is therefore $pp \to \tilde{g}\tilde{g}$, with a cross-section of 11 pb compared to the total cross-section of 27 pb. A selection of sparticle masses for Point 4 is given in table 14. The first thing to note is that, as for Point 3, the

Sparticle	Mass (GeV)	Sparticle	Mass (GeV)
$\tilde{q}$	914	$\tilde{g}$	582
$\tilde{\chi}_2^0$	150	$\tilde{\chi}_1^\pm$	149
$\tilde{\chi}_1^0$	80	h^0	113

Table 14: Some sparticle masses for SUGRA Point 4 using `ISAJET 7.31`.

two body decays $\tilde{\chi}_2^0 \to h^0\tilde{\chi}_1^0, Z^0\tilde{\chi}_1^0$ are kinematically not allowed. Therefore, the next to lightest neutralino decays as $\tilde{\chi}_2^0 \to \ell^+\ell^-\tilde{\chi}_1^0$ with a branching fraction of 6% for each lepton flavour. The invariant mass of OS SF leptons provides a precise measurement of the mass difference between the $\tilde{\chi}_2^0$ and $\tilde{\chi}_1^0$. This measurement will significantly constrain the model (it provides an indication of the $\tilde{\chi}_1^0$ mass and constrain the fundamental parameter $m_{1/2}$, as discussed in section 10.2). The gluino mainly decays as $\tilde{g} \to \tilde{\chi}_i qq$, where $\tilde{\chi}_i$ are both neutralinos and charginos. Thus events from $\tilde{g}\tilde{g}$ production often yield at least 4 jets in addition to the 6 jets from the $\tilde{\chi}_1^0$. The reconstruction of the $\tilde{\chi}_1^0$ in this type of events will therefore suffer from an even larger combinatorial background.

Since the neutralinos and charginos are light compared to the squarks and the gluino, there is a significant contribution from electroweak sparticle production. The cross-section for $pp \to \tilde{\chi}_i^\pm\tilde{\chi}_i^0$ is 3.52 pb. Production of $\tilde{\chi}_1^\pm\tilde{\chi}_2^0$ yields final states with three leptons through the decays

$$\begin{array}{rcl} \tilde{\chi}_2^0 & \to & \tilde{\chi}_1^0\ell^+\ell^- \\ & & \hookrightarrow jjj \end{array} \qquad (13)$$

and

$$\begin{array}{rcl} \tilde{\chi}_1^{\pm} & \rightarrow & \tilde{\chi}_1^0 \ell\nu \\ & & \hookrightarrow jjj \end{array} \tag{14}$$

The first decay has a branching ratio of 6% and the second one a branching ratio of 22%. There is no combinatorial background from gluino or squarks for this final state since all six jets come from the two $\tilde{\chi}_1^0$. For an integrated luminosity of $3 \cdot 10^4$ pb^{-1} 1300 events of this type are expected. The SM backgrounds are small once three leptons are required. The $\tilde{\chi}_1^0$ decay was studied at generator level for this type of events and the kinematics are given in table 15. The jets are well separated, but are very soft. Another strategy than

	hard	*soft*
$< p_T\ \tilde{\chi}_1^0 >$	112 GeV	68 GeV
$< p_T$ *quark-1*$>$	69 GeV	49 GeV
$< p_T$ *quark-2*$>$	32 GeV	25 GeV
$< p_T$ *quark-3*$>$	15 GeV	12 GeV
$<min(\Delta \mathrm{R})^{quarks} >$	0.63	0.88
$<max(\Delta \mathrm{R})^{quarks} >$	1.9	2.3

Table 15: The kinematics of $\tilde{\chi}_1^0$ decays with a $\tilde{\chi}_1^0$ mass of 80 GeV and for electroweak production of chargino/neutralino pairs at SUGRA Point 4.

reconstructing two $\tilde{\chi}_1^0$ decays from six jets therefore needs to be developed. With the six jets approach the jet threshold would need to be decreased below 15 GeV to maintain a reasonable reconstruction efficiency. A more promising possibility is to reconstruct the mass from a large jet cone containing all decay products. This strategy have been studied for W reconstruction in all hadronic decays [34, 35, 39]. It will, however, be more difficult to use such a method in SUSY events where two combinations need to be reconstructed with a few other hard jets present.

The above comments are generally valid for SUSY models with $\tilde{\chi}_1^0$ masses typically below 80-100 GeV. The direct reconstruction of the $\tilde{\chi}_1^0$ in the 3-jet channel is difficult in this case and different methods need to be investigated. A clear is although obtained through lepton final states. The low mass spectrum also ensures large cross-section so there will be many signals to look for. For most of these models, the $\tilde{\chi}_2^0$ two body decays to bosons are usually kinematically not allowed and the decay $\tilde{\chi}_2^0 \rightarrow \tilde{\chi}_1^0 \ell^+ \ell^-$ always has an appreciable branching ratio. Figure 35 shows the cross-section for the production of $\tilde{\chi}_2^0 \rightarrow \ell\ell\tilde{\chi}_1^0$ in SUSY events with the dashed lines indicating constant values of the $\tilde{\chi}_1^0$ mass.

11 Constraints on SUGRA Parameters

The measurement of several sparticles masses have been demonstrated in the previous sections for a SUSY model defined by the parameters of Point 5 in the case of R-parity

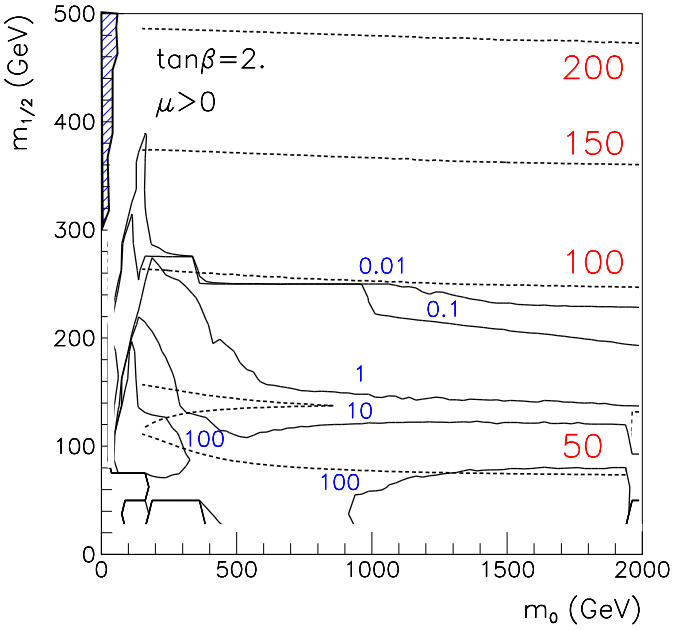

Figure 35: Plot in the $m_0 - m_{1/2}$-plane with production cross-section in pb for $\tilde{\chi}_2^0 \to \ell^+\ell^-\tilde{\chi}_1^0$ in SUSY cascade decays (solid lines, with small digits) and values of constant $\tilde{\chi}_1^0$ mass (dashed lines, with larg digits) The results are shown in the $m_0 - m_{1/2}$ plane for $\tan\beta$ =2.0 and μ >0.

Observable	Value (GeV)	Error (stat.) (GeV)	Error (sys.) (GeV)
edge $m_{\ell\ell}$	109	$\pm$0.30	$\pm$0.11
$m_{\tilde{\chi}_1^0}$	122	$\pm$3.1	$\pm$1.3
$m_{\tilde{\ell}_R}$	157	$\pm$5.1	$\pm$1.6
$m_{\tilde{\chi}_2^0}$	233	$\pm$4.1	$\pm$2.3
$m_{\tilde{q}_R}$	664	$\pm$30	$\pm$7
$m_{h^0}(h^0 \to \gamma\gamma)$	95	$\pm$0.3 requires 10^5 pb^{-1} of data	

Table 16: Expected measurements of SUSY particle masses and their uncertainties for a SUGRA model with baryonic R-parity violation.

violation. The expected results of these measurement are listed in table 16 together with the estimated errors.

The constraints on the SUGRA parameters from this fit are given in table 17. In the absence of a measurement of the h^0 boson mass, it is not possible to constrain $\tan\beta$. There is no sensitivity to A_0 since many different values of A_0 run to the same value at the weak scale due to a fixed point in the renormalization group evolution. The effect of A_0 on the particle spectrum is small except for the third generation. One should try to determine the weak scale parameters A_t, A_b, and A_τ. The solution $\mu < 0$ was discarded using the observed b-jet rate. However, if any of the λ'' that give $\tilde{\chi}_1^0$ decays to b-jets would be

Expected constraints		
Parameter	No $h^0 \to \gamma\gamma$ measurement	With $h^0 \to \gamma\gamma$ measurement
m_0	100^{+7}_{-5}	100^{+7}_{-5}
$m_{1/2}$	300 ± 6	300 ± 6
A_0	not sensitive	not sensitive
$\tan\beta$	$1.6 < \tan\beta < 4.0$	2.1 ± 0.1
μ	> 0	> 0

Table 17: Expected accuracy for extraction of fundamental SUGRA parameters for Point 5 with baryonic R-parity violation.

non-zero, this procedure would not work. More mass measurements of the SUSY masses at high luminosity will further constrain the model. The constraints obtained on the SUGRA parameters are similar to the ones for Point 5 with R-parity conserved [6].

The violation of R-parity added 45 couplings as free parameters to the SUGRA model, including 9 related to baryonic violation. If the experiment were to discover SUSY with R-parity violated, one would, of course, wish to determine which of the couplings contribute to the observed signal. The 3 couplings, λ''_{3jk}, with real top decays are not kinematically accessible. No less than 6 of the couplings, λ''_{ij3} give final states with b-jets which could be estimated using the observed b-jet rate. should increase significantly. Two other possible couplings λ''_{112} and λ''_{212}, remain where the former gives only light jets and the latter that was non-zero in this study give $\tilde{\chi}^0_1$ decays with one c-jet. More work is needed to study whether the role of different couplings can be untangled, but it is clear that the simple scenario with explicit breaking of R-parity due to only one non-zero coupling and no other decays than those of the $\tilde{\chi}^0_1$ affected, may eventually turn out to be quite unrealistic.

12 Conclusions

The studies reported in this note demonstrate that if supersymmetry exists with R-parity violated, it would be possible to discover it at LHC. There are, in fact, many semi-inclusive channels that can be used for an initial search. Moreover, if nature has chosen a model similar to Point 5, ATLAS will be able to measure several SUSY particle masses directly even for an integrated luminosity of only $3 \cdot 10^4$ pb^{-1}. One should note, though, that the calculation of the dominant background from QCD events with high jet multiplicities has significant theoretical uncertainties.

The jet multiplicity of SUSY events with hadronic $\tilde{\chi}^0_1$ decays is very high and many jets overlap resulting in a very challenging experimental scenario. However, it has been demonstrated in this study that the SUSY signal can be well reconstructed using two different jet finders and that the reconstructed masses and efficiencies do not depend too strongly on the details of the jet clustering, although the aspect of jet reconstruction has to be revisited in the case of lower values of the $\tilde{\chi}^0_1$ mass.

It was assumed in this study that one of the jets from the $\tilde{\chi}^0_1$ decay is charmed. This decreases the purity of events containing b-jets and, together with the increased jet multiplicity, severely deteriorates the reconstruction of the h^0 boson in the channel

$h^0 \to b\bar{b}$.

No attempt was made to measure any of the third generation scalar leptons or quarks. Their masses are sensitive to tanβ and A_0. It would therefore be useful to determine whether and how well they can be measured.

A global fit to the measurements of Point 5 provides constraints on the fundamental parameters of the SUGRA model to a precision of roughly 5%. Only measurements at low luminosity have been considered in this study and an extension to high luminosity should further improve the sparticle measurements and the constraints on the paramaters of the model.

The reconstruction technique used for Point 5 works also for Point 1 and Point 2. The particle spectra of Point 3 and Point 4 are much softer, which makes the $\tilde{\chi}_1^0$ reconstruction more difficult. The discovery of SUSY in these models is, however, guaranteed from multiple lepton signatures and fairly large cross-sections.

To summarise, a SUSY model with baryonic R-parity violation giving very different final state signatures compared to those previously studied has been considered. The conclusion of this study is that ATLAS will be able to perform precision measurements in the SUSY sector providing strong constraints on the fundamental model parameters.

Acknowledgements

This work started together with Mark Pearce, but unfortunately he could not pursue this study due to other commitments. I thank him for the many interesting discussions and the early work on this topic and valuable comments on this manuscript. Discussions with Giacomo Polesello has greatly improved the quality of this work and I am indebted to him for his encouragement. I am grateful for the many useful and stimulating discussions with Ian Hinchliffe, Frank Paige, Daniel Froidevaux, and Elzbieta Richter-Wąs. The comments on this manuscript from Per Carlson, Daniel Froidevaux, Bengt Lund-Jensen and Clark Lindsey are appreciated. Financial support from Claes Adelskölds minnesfond and the Swedish Natural Science Research Council is acknowledged.

References

[1] For SUSY reviews see: H.P. Nilles, *Phys. Rep.* **110** (1984) 1, H.E. Haber and G.L. Kane, *Phys. Rep.* **117** (1985) 75.

[2] I. Hinchliffe, F..E. Paige, G. Polesello, E. Richter-Wąs, ATLAS Internal Note, PHYS-No-107, October 1997.

[3] E. Richter-Wąs, D. Froidevaux, J. Söderqvist, ATLAS Internal Note, PHYS-No-108, October 1997.

[4] I. Hinchliffe, E. Nagy, F.E. Paige, M.D. Shapiro, J. Söderqvist, W. Yao, ATLAS Internal Note, PHYS-No-109, October 1997.

[5] F. Gianotti, ATLAS Internal Note, PHYS-No-110, October 1997.

[6] ATLAS Internal Note, PHYS-No-110, October 1997 G. Polesello, L. Poggioli, E. Richter-Wąs, J. Söderqvist, ATLAS Internal Note, PHYS-No-111, October 1997.

[7] A. Bartl, J. Söderqvist et al., *Supersymmerty at LHC*, Proceedings of the 1996 DPF/DPB Summer Study on High-Energy Physics, Snowmass, USA June 25 - July 12, (1996)693, available from: `http://www.slac.stanford.edu`.

[8] I. Hinchliffe, F.E. Paige, M.D. Shapiro, J. Söderqvist, and W. Yao, *Phys. Rev.* **D55** (1997) 5520.

[9] F. Paige and S. Protopopescu, in *Supercollider Physics*, p. 41, ed. D. Soper (World Scientific, 1986). H. Baer, F. Paige, S. Protopopescu and X. Tata, in *Proceedings of the Workshop on Physics at Current Accelerators and Supercolliders*, ed. J. Hewett, A. White and D. Zeppenfeld (Argonne National Laboratory, 1993).

[10] Scanned copies of all the transparencies from this workshop are available from: `http://www.cern.ch/Committees/LHCC/SUSY96.html`

[11] H. Baer, C-h. Chen and X. Tata, *Phys. Rev.* **D55** (191997) 1466.

[12] For a recent review see: G. Jungman et al., *Phys. Rep.* **267** (1996) 195.

[13] G. Bhattacharyya, hep-ph/9608415 (1996).

[14] H. Dreiner, hep-ph/9707435 (1997).

[15] L.J. Hall, M. Suzuki, *Nucl. Phys.* **B231** (1984) 419.

[16] A. Bartl et al., hep-ph/9612436

[17] J. Ellis et al. *Nucl. Phys.* **B373** (1992) 399.

[18] Reno et al. *Phys. Rev.* **D37** (1988) 3441.

[19] The decay $\tilde{\chi}_1^0 \to \ell\ell\nu$ is studied by E. Nagy and A. Mirea,, CPPM, Marseille, see ATLAS SUSY working group meeting 4 March 1998.

[20] T. Sjöstrand, Comp. Phys. Comm. **82**,(1994)74.

[21] G. Marchesini et al, Comp. Phys. Comm. **67** ,(1992)465. Used default Parton Distribution Function (MRS).

[22] E. Richter-Wąs, D. Froidevaux, L. Poggioli, ATLAS Internal Note, PHYS-NO-079, 1 March, 1996.

[23] See talk by D. Froidevaux in [10].

[24] I. Parkic, ATLAS Note in preparation, available from:
`http://wwwinfo.cern.ch/p/parkic/www/JetFinder/`

[25] ATLAS Collaboration, ATLAS Inner Detector, TDR, CERN/LHCC/97-16, ATLAS TDR 4, 30 April 1997.

[26] D. Cavalli et al, ATLAS Internal Note, PHYS-No-051, 22 December, 1994.

[27] Program code kindly made available by I. Gavrilenko. See for instance R.J. Barlow, Statistics, Wiley & Sons, 1989, p. 155.

[28] ATLAS collaboration: *ATLAS Calorimeter Performance*, CERN/LHCC/96-40, ATLAS TDR 1, 15 December 1996.

[29] H. Baer and M. Brhlik, *Phys. Rev.* **D53** (1996) 597

[30] E. Richter-Wąs, D. Froidevaux, ATLAS Internal Note, PHYS-No-104, July 1997.

[31] F. Abe et al., Fermilab-PUB-97/093-E, April 16, 1997.

[32] F. A. Berends and H. Kuijf, *Nucl. Phys.* **B353** (1991) 59.

[33] H. Baer et al., *Phys. Rev.* **D53** (1996) 6241.

[34] S. Zmushko et al., ATLAS Internal Note, PHYS-No-008, 3 November, 1992.

[35] S. Zmushko et al., ATLAS Internal Note, PHYS-No-103, 12 June, 1997.

[36] E. Richter-Wąs et al., ATLAS Internal Note, PHYS-No-074, 24 April, 1996.

[37] P. Janot, Talk given at EPS 1997, Jerusalem, transparencies available from: `http://www.cern.ch/hep97`

[38] J. Söderqvist, Proceedings of the 1996 DPF/DPB Summer Study on High-Energy Physics, Snowmass, USA, June 25 - July 12 (1996)715, available from: `http://www.slac.stanford.edu`.

[39] P. Savard, ATLAS Internal note, CAL-No-092, 6 May 1997.